IEEE Access
Multidisciplinary : Rapid Review : Open Access Journal

Received May 29, 2020, accepted June 2, 2020, date of publication June 10, 2020, date of current version July 2, 2020.

Digital Object Identifier 10.1109/ACCESS.2020.3001393

Dynamic Radar Network of UAVs: A Joint Navigation and Tracking Approach

ANNA GUERRA[1,2], (Member, IEEE), DAVIDE DARDARI[1], (Senior Member, IEEE), AND PETAR M. DJURIĆ[2], (Fellow, IEEE)

[1]Department of Electrical, Electronic, and Information Engineering "Guglielmo Marconi," University of Bologna, 40136 Bologna, Italy
[2]Department of Electrical and Computer Engineering, Stony Brook University, Stony Brook, NY 11794, USA

Corresponding author: Anna Guerra (anna.guerra3@unibo.it)

This work was received funding from the EU's H2020 research and innovation programme under the Marie Sklodowska-Curie project AirSens (grant no. 793581).

ABSTRACT Nowadays there is a growing research interest on the possibility of enriching small flying robots with autonomous sensing and online navigation capabilities. This will enable a large number of applications spanning from remote surveillance to logistics, smarter cities and emergency aid in hazardous environments. In this context, an emerging problem is to track unauthorized small unmanned aerial vehicles (UAVs) hiding behind buildings or concealing in large UAV networks. In contrast with current solutions mainly based on static and on-ground radars, this paper proposes the idea of a dynamic radar network of UAVs for real-time and high-accuracy tracking of malicious targets. To this end, we describe a solution for real-time navigation of UAVs to track a dynamic target using heterogeneously sensed information. Such information is shared by the UAVs with their neighbors via multi-hops, allowing tracking the target by a local Bayesian estimator running at each agent. Since not all the paths are equal in terms of information gathering point-of-view, the UAVs plan their own trajectory by minimizing the posterior covariance matrix of the target state under UAV kinematic and anti-collision constraints. Our results show how a dynamic network of radars attains better localization results compared to a fixed configuration and how the on-board sensor technology impacts the accuracy in tracking a target with different radar cross sections, especially in non line-of-sight (NLOS) situations.

INDEX TERMS Unmanned aerial vehicles, radar, navigation, target tracking, information gathering.

I. INTRODUCTION

The use of UAVs in densely inhabited areas like cities is expected to open an unimaginable set of new applications thanks to their low-cost and high flexibility for deployment. They can be useful in response to specific events, like for instance in natural disasters or terrorist attacks as an emergency network for assisting rescuers [1], or for extended coverage and capacity of mobile radio networks [2]. In fact, UAVs have been proposed as flying base stations for future wireless networks [3]–[6] because 5G and Beyond will be characterized by a massive density of nodes requiring high data rates and supporting huge data traffic [7]. This will require a much higher degree of network flexibility than in the past in order to smoothly and autonomously react to fast temporal and spatial variations of traffic demand. At the same time, the idea of having swarms of UAVs being accepted by the wide public might be challenging because of the possibility of their malicious use [8], [9]. In fact, an important problem is the possible presence of sinister UAVs that can hide behind buildings for illegal activities, e.g., terrorist attacks, or can blind UAV swarms to inhibit their functionality. The problem of fast, reliable, and autonomous detection and tracking of malicious UAVs is challenging and still an unsolved issue because most solutions would require the deployment of ad-hoc aerial or terrestrial radar or vision-based infrastructures that might not be economically sustainable or acceptable [10], [11].

Today, current technological solutions are mainly based on surface-sited (terrestrial) and fixed radars, as battlefield radars, bird detection radars, perimeter surveillance radars, or high-resolution short-range radars, adopted in critical areas (e.g., airports) (see [8]–[10], [12]–[14] and the references therein). The possibility of monitoring the movement of

The associate editor coordinating the review of this manuscript and approving it for publication was Derek Abbott.

This work is licensed under a Creative Commons Attribution 4.0 License. For more information, see https://creativecommons.org/licenses/by/4.0/

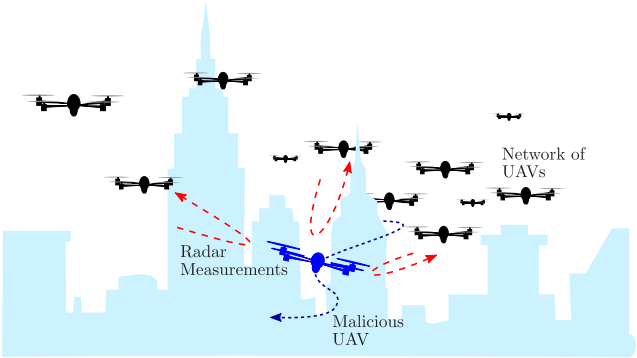

FIGURE 1. Pictorial representation of a DRN considered in this paper.

small-sized UAVs using a multi-functional airfield radar is considered in [13]. In [15]–[17], the detection and localization performance of frequency-modulated continuous-wave (FMCW) radar systems is discussed. In [14], a joint connectivity and navigation problem is considered when the radar receiver is mounted on UAVs while the transmitter is on the ground in a multi-static configuration. In [18], a network of UAVs is used to track ground vehicles.

Nevertheless, the tracking of a malicious UAV with conventional terrestrial radars poses some difficulties because the UAVs might be of small size and concealed within the UAV swarm, implying a low probability of being detected and tracked. Similar shortcomings are present with camera-based solutions, as in [11]. There a shortest path planning problem is considered for a group of UAVs, organized in a hierarchical network guided by a global planner, that should localize active emitters while simultaneously minimizing the distance from them. Vision systems also fail in NLOS conditions, for example when the target is hidden between buildings and is not directly "visible" by the swarm.

For these reasons, differently from the literature and from our previous works [19], [20], where usually radar sensor networks and UAVs are treated separately, this paper aims at introducing the concept of a monostatic dynamic radar network (DRN) consisting of UAVs carrying scanning radars of small sizes and weights, able to track a target and, simultaneously, adapt their formation-navigation control based on the quality of the signals backscattered by a non-cooperative (passive) flying target present in the environment. The considered network interrogates the surrounding via echoing signals, estimates and exchanges some target position-related information (e.g., ranging, bearing, and/or Doppler shifts), and jointly infers the target's current position and velocity. The proposed scenario is displayed in Fig. 1 where each UAV individually exchanges measurements with neighboring UAVs and takes navigation decisions on-the-fly in order to reduce the uncertainty on target tracking.

In order to realize the aforementioned UAV-DRN, on-board radar technology should be chosen according to the UAV size and maximum payload. To this end, a promising solution might be to use millimeter wave (mm-wave) radar technology because of the possibility to miniaturize it for an on-board system and for its ranging accuracy and precision thanks to its larger available bandwidth [21]–[23]. Furthermore, a MIMO solution can be employed due to its small size, which will result in a highly directional radiation pattern (up to 1-degree angular accuracy [21]). For example, in [22], FMCW radar sensors working at 77 GHz are proposed for automotive applications. Moreover, when considering a target whose size is comparable to that of a mini/micro-UAV, FMCW scanning radars are usually preferred compared to pulse radars that perform poorly in localizing small radar cross sections (RCSs) [13]. For this reason, some research activities have focused on the assessment of the RCS values of UAVs and their impact on the detection performance [8], [24], [25]. However, how the target RCS affects tracking accuracy and navigation performance is an open issue.

Another challenge in the realization of a UAV-DRN is the design of optimized paths for the UAVs to track malicious targets in the best possible way. The optimization of UAV trajectories has been the subject of numerous research studies [26]–[38]. In regard to control design, many works in the literature have focused on optimal sensor/anchor placement [26], [38], while others tackle the problem from an optimal control point-of-view [37]. Among other approaches, information-seeking optimal control (e.g., strategies driven by Shannon or Fisher information measures) has been extensively investigated for localization and tracking applications [29]–[31], [33]–[36], [38], [39]. For example, an analysis of the best network geometry was performed in [38], The analysis was based on a Fisher information metric for a team of collaborative UAVs used to track on-ground targets, but, in this solution, the target estimation algorithm and the trajectory design were not optimized together with the swarm formation. Moreover, the Fisher Information Matrix (FIM) derived in this work did not consider prior information or motion models. Further, these approaches usually do not account for the dynamics of the environment (they define the entire paths *a priori*), and they do not consider NLOS biases or the effect of the target's RCS in the measurement model. Thus, they are not suitable for our scenario where the UAVs have to adjust their trajectories in real-time and in accordance to the movements of the unauthorized flying target that can be of small dimension (mini/micro UAV).

Given this background, the aim of this paper is to study a UAV DRN as a cooperative radar sensing network for jointly tracking a non-authorized UAV in real-time and with high-accuracy and for smartly navigating the environment in order to reduce the correspondent tracking error (via multi-hop exchange of information). The design of DRNs, where the sensors and the target are flying (hence, mobile) poses new challenging issues because of their reconfigurability and mobility, but also offers an unprecedented level of flexibility for target tracking systems thanks to an increased degrees of freedom. Since not all the paths are the same

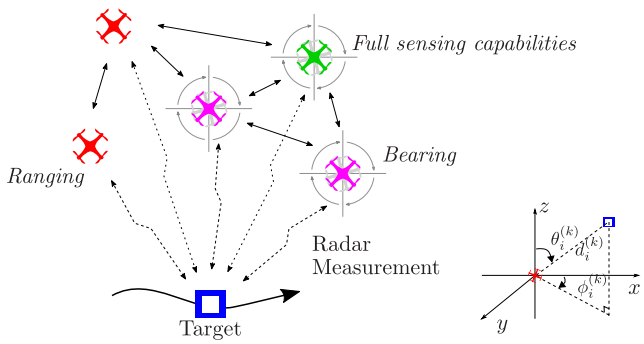

FIGURE 2. A UAV network, where different groups of UAVs acquire radar measurements. On the left, starting from the environment echo, the red UAVs measure ranging information, the magenta the direction of arrival, and the green has full sensing capabilities (including the possibilities of inferring Doppler shifts). On the right, there is the used coordinate system.

from an information gathering point-of-view, the navigation will be formulated as a 3D optimization problem where an information-theoretic cost function permits to combine the *a priori* information given by the history of measurements and the contributions brought by the currently acquired data, that can be delayed by the number of hops (and, hence, they can be aged). The impact of the RCS of small target (e.g., micro-UAV) will be taken into consideration in the measurement noise model, and in assessing the estimation accuracy.

The rest of the paper is organized as follows: Sec. II describes the problem, Sec. III reports details about the radar signal model and the tracking of a non-cooperative UAV, Sec. IV derives the cost function for optimizing the UAV navigation, Sec. V provides a possible solution for the optimization problem, and Sec. VI describes some simulations results.

Notation: Vectors and matrices are denoted by bold lowercase and uppercase letters, respectively; $[\mathbf{X}]_{ij}$ denotes the (i,j)th entry of the matrix $\mathbf{X}$; $f(x)$ symbolizes a probability density function (pdf) of a continuous random variable x; $f(x|z)$ is the conditional distribution of x given z; $\mathbf{x} \sim \mathcal{N}(\boldsymbol{\mu}, \boldsymbol{\Sigma})$ means that $\mathbf{x}$ is distributed according to a Gaussian pdf with mean $\boldsymbol{\mu}$ and covariance matrix $\boldsymbol{\Sigma}$; $x \sim \mathcal{U}[a,b]$ denotes that x is a uniform random variable with support $[a,b]$; $\mathbb{E}\{\cdot\}$ represents the expectation of the argument; $[\cdot]^{\mathsf{T}}$ denotes transposition of the argument. Finally, $\mathbf{I}_{n\times m}$ and $\mathbf{0}_{n\times m}$ indicate the identity and zero matrices of $n \times m$ size, respectively.

II. PROBLEM STATEMENT

We consider a DRN of N UAVs acting as mobile reference nodes (that is, with *a priori* known positions[1]) that navigate through an outdoor environment in order to optimize the accuracy in tracking the position, $\mathbf{p}_0^{(k)}$, and the velocity, $\mathbf{v}_0^{(k)}$, of a moving non-cooperative target.[2] The time is discrete and indexed with the symbol k.

The mobility model of UAVs can be considered deterministic as the UAVs are flying outdoors (and, hence, they access the GPS signal with a high degree of accuracy) and, at each time instant, the next position of the ith UAV is given by $\mathbf{p}_i^{(k+1)} = \varphi\left(\mathbf{p}_i^{(k)}, \mathbf{u}_i^{(k)}\right)$, where $\varphi(\cdot)$ is the transition function, $\mathbf{p}_i^{(k)} = \left[x_i^{(k)}, y_i^{(k)}, z_i^{(k)}\right]^{\mathsf{T}}$ is the position of the ith UAV at time instant k, and $\mathbf{u}_i^{(k)} = \left[u_{\mathsf{x},i}^{(k)}, u_{\mathsf{y},i}^{(k)}, u_{\mathsf{z},i}^{(k)}\right]^{\mathsf{T}} = g\left(v_i^{(k)}, \Psi_i^{(k)}, \Theta_i^{(k)}\right)$ is the control signal that the ith UAV computes on its own for accurate tracking of the target [27]. The magnitude of the speed, the heading and the tilt angles are denoted by $v_i^{(k)}$, $\Psi_i^{(k)}$, and $\Theta_i^{(k)}$, respectively. In particular, the update of the position is given by

$$\begin{bmatrix} x_i^{(k+1)} \\ y_i^{(k+1)} \\ z_i^{(k+1)} \end{bmatrix} = \begin{bmatrix} x_i^{(k)} + u_{\mathsf{x},i}^{(k)} \\ y_i^{(k)} + u_{\mathsf{y},i}^{(k)} \\ z_i^{(k)} + u_{\mathsf{z},i}^{(k)} \end{bmatrix} = \begin{bmatrix} x_i^{(k)} + v_i^{(k)} \cos\left(\Psi_i^{(k)}\right) \sin\left(\Theta_i^{(k)}\right) \Delta t \\ y_i^{(k)} + v_i^{(k)} \sin\left(\Psi_i^{(k)}\right) \sin\left(\Theta_i^{(k)}\right) \Delta t \\ z_i^{(k)} + v_i^{(k)} \cos\left(\Theta_i^{(k)}\right) \Delta t \end{bmatrix}, \quad (1)$$

with Δt being the time interval between k and $k+1$. To make the model more realistic, three constraints are added to impose the minimum and maximum speed and a maximum turn rate in both azimuthal and elevation planes [29], that are

$$\begin{cases} v_{\mathsf{min}} \le v_i^{(k)} \le v_{\mathsf{max}}, \\ \left|\Psi_i^{(k)} - \Psi_i^{(k-1)}\right| \le \Psi_{\mathsf{max}}, \\ \left|\Theta_i^{(k)} - \Theta_i^{(k-1)}\right| \le \Theta_{\mathsf{max}}, \end{cases} \quad (2)$$

where v_{min} and v_{max} are the minimum and maximum UAV speeds, respectively, and Ψ_{max} and Θ_{max} are the turn rate limits, respectively. The geometry of the system in depicted in Fig. 2.

On the other hand, the target state vector at time instant k is defined as $\mathbf{s}^{(k)} = \left[\left(\mathbf{p}_0^{(k)}\right)^{\mathsf{T}}, \left(\mathbf{v}_0^{(k)}\right)^{\mathsf{T}}\right]^{\mathsf{T}}$, where the target position expressed in relation to the ith UAV position at time instant k is

$$\mathbf{p}_0^{(k)} = \begin{bmatrix} x_0^{(k)} \\ y_0^{(k)} \\ z_0^{(k)} \end{bmatrix} = \begin{bmatrix} x_i^{(k)} + d_i^{(k)} \sin\left(\theta_i^{(k)}\right) \cos\left(\phi_i^{(k)}\right) \\ y_i^{(k)} + d_i^{(k)} \sin\left(\theta_i^{(k)}\right) \sin\left(\phi_i^{(k)}\right) \\ z_i^{(k)} + d_i^{(k)} \cos\left(\theta_i^{(k)}\right) \end{bmatrix}, \quad (3)$$

where $d_i^{(k)} = \|\mathbf{p}_0^{(k)} - \mathbf{p}_i^{(k)}\|_2$ is the distance between the ith UAV and the target at time instant k,

[1]The UAV positions are considered known with centimeter accuracy, for instance, provided by visual aided GNSS/INS sensors, so that the UAV localization error can be considered negligible with respect to the one associated to the target [40].

[2]In the sequel, we only consider a single-target tracking problem. A possible extension to a multitarget scenario would require a clustering process for assigning the target to respective sub-teams of UAVs as, for example, proposed in [41].

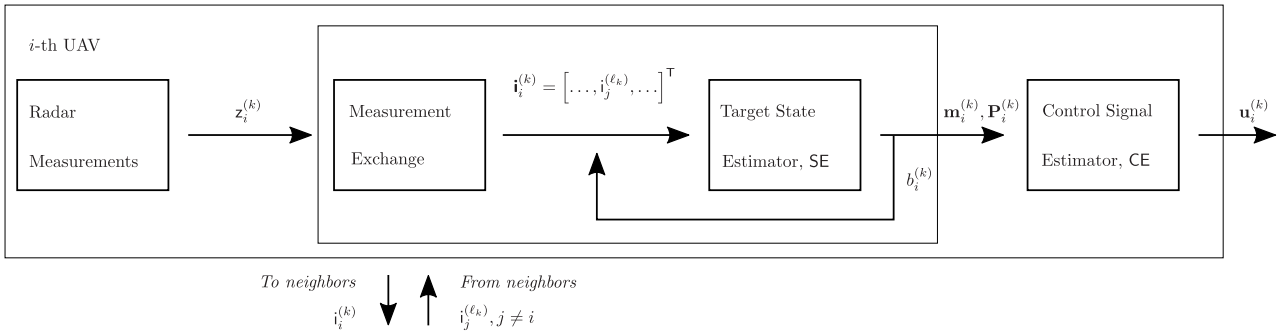

FIGURE 3. A block-diagram for decentralized joint tracking and navigation at the ith UAV.

and $\mathbf{v}_0^{(k)} = \left[v_{x,0}^{(k)}, v_{y,0}^{(k)}, v_{z,0}^{(k)}\right]^T$ is its velocity. The state evolves according to the following dynamic model,

$$\mathbf{s}^{(k+1)} = \mathbf{A}^{(k)}\,\mathbf{s}^{(k)} + \mathbf{q}^{(k)}, \tag{4}$$

where $\mathbf{A}^{(k)}$ is the transition matrix, which is assumed known, and $\mathbf{q}^{(k)} \sim \mathcal{N}\left(\mathbf{0}, \mathbf{Q}^{(k)}\right)$ is the process noise.

All UAVs perform radar measurements with respect to the target, and starting from the acquired data, they can estimate Doppler shifts, ranging and/or bearing from which the position and the velocity of the target can finally be estimated at each time step (two-step localization) through cooperation [42]. In fact, starting from the radar received signals, the Doppler shift and ranging information can be inferred given the beat frequency estimation [17]; whereas the direction-of-arrival (DOA) can be associated with the antenna steering direction. More specifically, UAV rotations might be exploited to point the on-board radar antenna in different angular directions and to form a received signal strength (RSS) pattern after each rotation as in [43]. As an alternative, one may consider a MIMO radar system with electronic beamforming capabilities [12]. Hence, each UAV can process the collected measurements in different ways: We indicate with $\mathcal{N}_{\mathsf{r}}$ the set of UAVs that exclusively acquire ranging estimates, with $\mathcal{N}_{\mathsf{d}}$ the group that only works with Doppler shifts, with $\mathcal{N}_{\mathsf{b}}$ the set operating on bearing-only data, and with $\mathcal{N}_{\mathsf{j}}$ the set that has access to all the types of measurements. The network composed of UAVs with heterogeneous capabilities is indicated with $\mathcal{N} = \mathcal{N}_{\mathsf{r}} \cup \mathcal{N}_{\mathsf{d}} \cup \mathcal{N}_{\mathsf{b}} \cup \mathcal{N}_{\mathsf{j}}$, where $\cup$ is the union operator.

In accordance with Fig. 3, the ith UAV performs the following steps at time instant k:

Measurement step: The first task is to retrieve state-related information from radar measurements, i.e., from the signal backscattered by the environment where the malicious target navigates. In Fig. 3, we indicate with $\mathsf{z}_i^{(k)}$ the measurements inferred by the ith UAV at time instant k;

Communication step: The ith UAV communicates this information to the neighbors together with its own position $\left(\text{defined as } \mathsf{i}_i^{(k)} = \left[\mathsf{z}_i^{(k)}, \mathbf{p}_i^{(k)}\right]\right)$, and it receives back the same data from neighboring UAVs via multi-hop propagation, i.e., $\mathsf{i}_j^{(\ell_k)} = \left[\mathsf{z}_j^{(\ell_k)}, \mathbf{p}_j^{(\ell_k)}\right]$, where ℓ_k is a time index accounting for the delay due to multi-hops [19], [44], [45]. Each node can directly communicate with its neighbors within a radius of length $r_{\max}$, while for greater distances, the information is delayed by $h_{ij}^{(k)}$ time slots, equal to the number of hops between the ith and jth UAV at instant k. We indicate with $\mathcal{N}_{\mathsf{nb},i}^{(k)}$ the set of neighbors of the ith UAV at time instant k. Due to multi-hop propagation, the information obtained at each UAV can be aged, preventing an updated view of the network. Finally, we gather all the acquired data in $\mathbf{i}_i^{(k)}$, which is the vector that contains the measurements and locations of the ith UAV and its neighbors.

Target Tracking: Given the measurements and the positions of the other UAVs, the presence of a malicious target can be detected and its state can be tracked by each UAV. A Bayesian estimator can be used to compute the *a-posteriori* probability distribution of the target state given the acquired information $\left(\text{the belief is denoted with } b_i^{(k)}\left(\mathbf{s}^{(k)}\right) \text{ in Fig. 3}\right)$. In our case, we adopt an Extended Kalman Filter (EKF) algorithm to compute the Gaussian belief of the state as $b_i^{(k)}\left(\mathbf{s}^{(k)}\right) = f\left(\mathbf{s}^{(k)} | \mathbf{i}_i^{(1:k)}\right) \overset{\text{EKF}}{=} \mathcal{N}\left(\mathbf{m}_i^{(k)}, \mathbf{P}_i^{(k)}\right)$, where $\mathbf{m}_i^{(k)}$ and $\mathbf{P}_i^{(k)}$ are the conditional mean vector and the covariance matrix of the state and $\mathbf{i}_i^{(1:k)}$ is the acquired information by the ith UAV up to time instant k. The EKF filter algorithm produces estimates that minimize the mean-squared estimation error conditioned on the history of acquired information. Consequently, the estimate of the state at time k, $\hat{\mathbf{s}}_i^{(k)}$, is defined as the conditional mean $\hat{\mathbf{s}}_i^{(k)} = \mathbf{m}_i^{(k|k)} = \mathbb{E}\left\{\mathbf{s}^{(k)} | \mathbf{i}_i^{(1:k)}\right\}$.[3] With reference to Fig. 3, we can write

$$\begin{aligned} \hat{\mathbf{s}}_i^{(k)} &= \mathsf{SE}\left(\mathbf{i}_i^{(k)}, b_i^{(k-1)}\left(\mathbf{s}^{(k-1)}\right)\right) \\ &\overset{\text{EKF}}{=} \mathsf{SE}\left(\mathbf{i}_i^{(k)}, \mathbf{m}_i^{(k-1)}, \mathbf{P}_i^{(k-1)}\right), \end{aligned} \tag{5}$$

with $\mathsf{SE}(\cdot)$ being a function describing the state estimator. Subsequently, an approach based on diffusion of information [47] can follow to further enhance the estimation accuracy.

UAV control step The last step is the control signal estimation by the ith agent that will allow the UAV to reach its

[3]The notation in the superscript $^{(n|m)}$ refers to the estimate at the nth time instant conditioned to information acquired until time instant m [46].

next position, $\mathbf{p}_i^{(k+1)}$, according to a given command, $\mathbf{u}_i^{(k)}$. Since the quality of the measurements depends on the DRN geometry and target position, the control law should properly change the UAV formation and position in order to maximize the quality of the tracking process and, at the same time, take into account physical constraints (e.g., obstacles). For this reason, at each time step, each UAV searches for the next UAV formation that minimizes an information-theoretic cost function at the next time instant, that can be written as [4]

$$\left(\mathbf{L}_i^{(k+1)}\right)^{\star} = \text{argmin}_{\mathbf{L}_i^{(k+1)}} \ \mathcal{C}\left(\mathbf{J}_i^{(k)}\left(\hat{\mathbf{p}}_{0;i}^{(k+1|k)}, \mathbf{L}_i^{(k+1)}\right)\right), \quad (6)$$

where $\mathbf{L}_i^{(k)} = \left[\ldots, \mathbf{p}_j^{(\ell_k)}, \ldots\right]^{\mathsf{T}}$, $j \in \mathcal{N}_{\mathsf{nb},i}^{(k)}$, is the vector containing the locations of UAVs that are neighbors of the ith UAV at time instant k $\left(\text{those belonging to the set } \mathcal{N}_{\mathsf{nb},i}^{(k)}\right)$, $\ell_k = k - h_{ij}^{(k)} + 1$ is the time instant associated with the exchanged information due to multi-hops, $\mathcal{C}(\cdot)$ is a function that will be defined in the sequel, $\mathbf{J}_i^{(k)}$ is the cost function also defined in the next, and $\hat{\mathbf{p}}_{0;i}^{(k+1|k)} = \left[\hat{\mathbf{s}}_i^{(k+1|k)}\right]_{1:3}$ is the predicted target position where $\hat{\mathbf{s}}_i^{(k+1|k)}$ is derived during the *prediction step* of (5), i.e., using a transition model.

Then, recalling (1), the control signal of the ith UAV that satisfies (6) is given by $\mathbf{u}_i^{(k)} = \left[\left(\mathbf{L}_i^{(k+1)}\right)^{\star}\right]_i - \mathbf{p}_i^{(k)}$, where $[\cdot]_i$ is an operator that picks the ith entry of the optimal formation in (6).

According to the D-optimality criterion described in [33], we choose the following cost function:

$$\mathcal{C}\left(\mathbf{J}_i^{(k)}\left(\mathbf{p}_0^{(k)}, \mathbf{L}_i^{(k)}\right)\right) = -\ln\det\left(\mathbf{J}_i^{(k)}\left(\mathbf{p}_0^{(k)}; \mathbf{L}_i^{(k)}\right)\right), \quad (7)$$

where $\det(\cdot)$ is the determinant operator, and $\mathbf{J}_i^{(k)}\left(\mathbf{p}_0^{(k)}; \mathbf{L}_i^{(k)}\right)$ is the *information matrix* of the target's location as a function of the current and previous locations of the neighboring UAVs. Following the same principle as in [29], we consider the posterior covariance matrix in its inverse (information) form as

$$\mathbf{J}_i^{(k)}\left(\mathbf{p}_0^{(k)}; \mathbf{L}_i^{(k)}\right) = \left[\left(\mathbf{P}_i^{(k|k)}\right)^{-1}\right]_{11}, \quad (8)$$

where the operator $[\cdot]_{11}$ picks the sub-matrix relative to the target position, and with the covariance matrix defined as

$$\mathbf{P}_i^{(k|k)} = \begin{bmatrix} \mathbf{P}_{\mathsf{pp},i}^{(k|k)} & \mathbf{P}_{\mathsf{pv},i}^{(k|k)} \\ \mathbf{P}_{\mathsf{vp},i}^{(k|k)} & \mathbf{P}_{\mathsf{vv},i}^{(k|k)} \end{bmatrix}, \quad (9)$$

whose diagonal contains the variances of the position and the velocity estimates. The cost function defined in (7) requires knowledge of the actual target position which is the unknown parameter to be estimated, and for this reason (6) is evaluated at the predicted position estimate for time instant $k+1$ computed by the ith UAV at time instant k.

[4]Here we suppose that the connectivity between nodes is unaltered from time instant k to $k+1$, meaning that the ith UAV solves the optimization problem by assuming that, at $k+1$, it will communicate with the same neighbors.

Finally, we consider that the problem is subjected to the following set of constraints:

$$\begin{cases} d_{ij}^{(k)} \geq d_{\mathsf{U}}^{*}, \ d_i^{(k)} \geq d_{\mathsf{T}}^{*}, \ \mathcal{T}_i \cap \mathcal{O} = \varnothing, \\ v_{\mathsf{min}} \leq v_i^{(k)} \leq v_{\mathsf{max}}, \\ |\Psi_i^{(k+1)} - \Psi_i^{(k)}| \leq \Psi_{\mathsf{max}}, \\ |\Theta_i^{(k+1)} - \Theta_i^{(k)}| \leq \Theta_{\mathsf{max}}, \end{cases} \quad (10)$$

for $i, j = 1, \ldots, N$, and where $d_{ij}^{(k)}$ is the inter-UAV distance, d_{U}^{*} is the anti-collision safety distance among UAVs, d_{T}^{*} is the safety distance with respect to the target, $\mathcal{T}_i$ is the set of feasible position points of the trajectory of the ith UAV, and $\mathcal{O}$ is the set of obstacles present in the environment from which the UAVs should keep a safety distance equal to d_{O}^{*}.

III. UAV-TARGET TRACKING

The target tracking aims to estimate the state of the target (e.g., its position and velocity) starting from the received echo signals. In this section, we briefly recall the signal model used by a FMCW radar that might be integrated in the UAV payload and, then, we focus on a Bayesian filtering method for target tracking. More specifically, we adopt an EKF as a tool to solve the tracking problem thanks to its capability of dealing with heterogeneous measurements, statistical characterization of uncertainties, and UAV mobility models.

A. EXAMPLE OF SIGNAL MODEL FOR ON-BOARD FMCW RADAR

A widely used radar technology for UAVs is the FMCW radar that, differently from pulse radars, interrogates the environment with a signal linearly modulated in frequency (namely, chirp). Sometimes, in order to increase the signal-to-noise ratio (SNR) and infer Doppler shift measurements, multiple chirps can be transmitted in a fixed time window (chirp train). Once the signal is received back by the radar, it is combined with a template of the transmitted waveform by a mixer. As a result, different target-related parameters, such as ranging and Doppler shifts, can be inferred by processing the frequency and phase information of the signal at the output of this mixer. In particular, to retrieve velocity information, it is possible to rely on phase differences between different received chirps, or, directly, on Doppler-shift estimates. If the FMCW radar consists of multiple transmitting and receiving antennas (MIMO radar), the angle-of-arrival can be estimated through the measurement of phase differences between the antennas. Another possibility is to exploit the UAV rotations: by rotating the on-board antenna towards ad-hoc steering directions, the direction of arrival can be inferred by considering the maximum power of the received echoes.

A promising solution for UAV integration is to operate at millimeter-waves so that FMCW radars can be miniaturized and equipped with multiple antennas. By working at high frequencies, a resolution smaller than a millimeter can be obtained thanks to the higher available bandwidth, up to 4 GHz at 77 GHz. Example of FMCW for UAVs can be found in [12] and the references therein.

For the following analysis and in order to derive a suitable observation model for the tracking algorithm, it is important to characterize the noise uncertainties of the ranging, bearing, and Doppler shift estimates as inferred by the radar. To this end, the Cramér-Rao lower bound (CRLB) expression, which can be viewed as the minimum variance achievable by an unbiased estimator, can be considered for ranging and Doppler shift estimates, given by [48], [49]

$$\mathrm{var}\left(d_i^{(k)}\right) \geq \frac{3}{2}\left(\frac{2\,c}{\gamma}\right)^2 \frac{1}{(2\,\pi\,B_i)^2\ \mathsf{SNR}_i^{(k)}}, \tag{11}$$

$$\mathrm{var}\left(f_{\mathsf{d},i}^{(k)}\right) \geq \frac{1}{(2\,\pi)^2}\frac{6}{T_i^2\ \mathsf{SNR}_i^{(k)}}, \tag{12}$$

where $T_i = \tau_i\, M_i$ is the observation time, τ_i is the time sweep of a single sawtooth, B_i is the frequency sweep, M_i is the number of chirps (processing gain), $\gamma = 4$ is the path-loss exponent for two-way (radar) channel, c is the speed-of-light, and the SNR is defined as

$$\mathsf{SNR}_i^{(k)} = \frac{\lambda^2\, P_{\mathsf{t}}\, G^2\left(\Theta_b\right)}{(4\pi)^3\ P_{\mathsf{n}}} \cdot \frac{\rho}{\left(d_i^{(k)}\right)^{\gamma}} = \mathsf{SNR}_0 \cdot \frac{\rho}{\left(d_i^{(k)}\right)^{\gamma}}, \tag{13}$$

where ρ is the target RCS, SNR_0 is the SNR evaluated at $d_0 = 1$ m and $\rho_0 = 1$ m^2, λ is the wavelength, P_{t} is the transmitted power, $G\left(\Theta_b\right)$ is the antenna gain pointing at $\Theta_b = (\theta_b, \phi_b)$, $P_{\mathsf{n}} = N_0\, B_i$ is the noise power with $N_0 = \kappa_{\mathsf{b}}\, T_0\, F$, κ_{b} is the Boltzmann constant, T_0 is the receiver temperature, and F is the receiver noise figure.

On the other hand, for the bearing case, we suppose that the noise uncertainty (in terms of standard deviation) is constant in the azimuthal and elevation planes and coincides with the Half Power Beamwidth (HPBW) of the on-board antenna.

B. OBSERVATION MODEL

As described in the previous section, starting from the received signal echoes, each UAV estimates information about the target state, e.g., the distance and angle from the target or the Doppler shift. Subsequently, such information is exchanged between UAVs via multi-hops together with the UAV positions. At the end of this communication step, each UAV puts together the gathered information, exploitable for target tracking in a vector. Let $\mathbf{i}_i^{(k)} = \left[\ldots, \mathsf{i}_j^{(\ell_k)}, \ldots\right]^{\mathsf{T}}$ be the information available to the ith UAV at time instant k, where the generic element $\mathsf{i}_j^{(\ell_k)} = \left[\mathsf{z}_j^{(\ell_k)}, \mathbf{p}_j^{(\ell_k)}\right]^{\mathsf{T}}$, with $j \in \mathcal{N}_{\mathsf{nb},i}^{(k)}$, contains the radar estimates and the position of the jth neighboring UAV delayed due to the multi-hop connection with the ith agent. The generic radar measurement can be written as

$$\mathsf{z}_i^{(k)} = \mathsf{l}_i^{(k)}\, o_i^{(k)} + \left(1 - \mathsf{l}_i^{(k)}\right) w_i^{(k)}, \tag{14}$$

where $\mathsf{l}_i^{(k)}$ is a flag indicating the presence (if any) of a line-of-sight (LOS) link between the ith UAV and the target, and $w_i^{(k)}$ is an outlier term due to the presence of multipath components or extremely noisy measurements [50]. The first term in (14) contains information about the target state, that is

$$o_i^{(k)} = h_i^{(k)}\left(\mathbf{s}^{(k)}\right) + n_i^{(k)}, \tag{15}$$

where $h_i^{(k)}$ is a function that relates the data to the target state and whose expression depends on the UAV sensing and processing capabilities, i.e.,

$$h_i^{(k)} = \begin{cases} \frac{\gamma}{2} d_i^{(k)} = \frac{\gamma}{2}\left\|\mathbf{p}_0^{(k)} - \mathbf{p}_i^{(k)}\right\|_2, & \text{if } i \in \mathcal{N}_{\mathsf{r}} \vee \mathcal{N}_{\mathsf{j}}, \\ \phi_i^{(k)} = \tan^{-1}\left(y_{0i}^{(k)}/x_{0i}^{(k)}\right), & \text{if } i \in \mathcal{N}_{\mathsf{b}} \vee \mathcal{N}_{\mathsf{j}}, \\ \theta_i^{(k)} = \cos^{-1}\left(z_{0i}^{(k)}/d_i^{(k)}\right), & \text{if } i \in \mathcal{N}_{\mathsf{b}} \vee \mathcal{N}_{\mathsf{j}}, \\ f_{\mathsf{d},i}^{(k)} = \left(\gamma\, v_{\mathsf{rad},i}^{(k)}/2\,\lambda\right), & \text{if } i \in \mathcal{N}_{\mathsf{d}} \vee \mathcal{N}_{\mathsf{j}}, \end{cases} \tag{16}$$

where $d_i^{(k)}, \phi_i^{(k)}, \theta_i^{(k)}$, and $f_{\mathsf{d},i}^{(k)}$ are the actual distance, azimuth, elevation, and Doppler shift between the ith UAV and the target, $v_{\mathsf{rad},i}^{(k)}$ is the radial velocity, $\vee$ is the *or*-operator, and $x_{0i}^{(k)} = x_0^{(k)} - x_i^{(k)}$, $y_{0i}^{(k)} = y_0^{(k)} - y_i^{(k)}$, and $z_{0i}^{(k)} = z_0^{(k)} - z_i^{(k)}$.

The measurement noise in (15) is modeled as $n_i^{(k)} \sim \mathcal{N}\left(0, \left(\sigma_i^{(k)}\right)^2\right)$, where, in accordance with the type of measurement, the ranging and Doppler shift variances are described by the CRLB as in (11), that can be reformulated as

$$\left(\sigma_{\mathsf{r},i}^{(k)}\right)^2 = \sigma_{\mathsf{r},0}^2 \frac{\left(d_i^{(k)}\right)^{\gamma}}{\rho}, \quad \left(\sigma_{\mathsf{d},i}^{(k)}\right)^2 = \sigma_{\mathsf{d},0}^2 \frac{\left(d_i^{(k)}\right)^{\gamma}}{\rho}, \tag{17}$$

where $\sigma_{\mathsf{r},0}^2$ and $\sigma_{\mathsf{d},0}^2$ are the variances at the reference distance $d_i^{(k)} = 1$ m and with a target RCS of $\rho = 1$ m^2. On the contrary, the bearing noise variance is constant with respect to the distance and the target RCS, and $\sigma_{\mathsf{b},0}^2$ is related to the radar HPBW, as previously stated.

Eq. (14) can be written in vector form as

$$\mathbf{z}_i^{(k)} = \mathbf{l}_i^{(k)} \odot \left(\mathbf{h}_i^{(k)}\left(\mathbf{s}^{(k)}\right) + \mathbf{n}_i^{(k)}\right) + (1 - \mathbf{l}_i^{(k)}) \odot \mathbf{w}_i^{(k)}, \tag{18}$$

where $\odot$ is the Hadamard product, and the noise can be described as $\mathbf{n}_i^{(k)} \sim \mathcal{N}\left(\mathbf{0}, \mathbf{R}_i^{(k)}\right)$ with a covariance matrix given by $\mathbf{R}_i^{(k)} = \mathrm{diag}\left(\ldots, \left(\sigma_j^{(\ell_k)}\right)^2, \ldots\right)$.

C. UAV-TARGET TRACKING

Starting from the transition and measurement model previously described, each UAV can perform tracking to estimate the state of the target. Within this framework, the main goal of each UAV is to infer the full joint posterior probability of the state at time instant k, $\mathbf{s}^{(k)}$, given the available information up to the current time instant, namely $\mathbf{i}_i^{(1:k)}$.

In this context, it is possible to define a probabilistic state-space Markovian model by considering the following statistical models:

- *Measurement model*. It describes how the state is related to the available information by the likelihood $f\left(\mathbf{i}_i^{(k)}|\mathbf{s}^{(k)}\right) = f\left(\mathbf{z}_i^{(k)}|\mathbf{s}^{(k)}\right)$, defined by the statistical measurement model in (18);
- *State transition model*. It describes how the state evolves in time, in accordance with the dynamic model in (4) and given by $f\left(\mathbf{s}^{(k)}|\mathbf{s}^{(k-1)}\right)$.

Given this state-space model, an EKF approach can be used because the observation functions in (14) are non-linear and the noises are Gaussian distributed. In this case, each UAV performs the two main steps of the EKF algorithm: (i) A *prediction step* within which each UAV computes the predictive information $\left(\mathbf{m}_i^{(k|k-1)}, \mathbf{P}_i^{(k|k-1)}\right)$ given a model for the target mobility as in (4); and (ii) An *update step* for updating the mean and covariance $\left(\mathbf{m}_i^{(k|k)}, \mathbf{P}_i^{(k|k)}\right)$ once a new measurement becomes available. The Jacobian matrix $\nabla\mathbf{h}_i^{(k)}$ is given by

$$\nabla\mathbf{h}_i^{(k)} = \begin{bmatrix} \nabla_{\mathbf{p}_0^{(k)}}\left(\mathbf{h}_{\mathsf{r},i}^{(k)}\right) & \mathbf{0} \\ \nabla_{\mathbf{p}_0^{(k)}}\left(\mathbf{h}_{\phi,i}^{(k)}\right) & \mathbf{0} \\ \nabla_{\mathbf{p}_0^{(k)}}\left(\mathbf{h}_{\theta,i}^{(k)}\right) & \mathbf{0} \\ \nabla_{\mathbf{p}_0^{(k)}}\left(\mathbf{h}_{\mathsf{d},i}^{(k)}\right) & \nabla_{\mathbf{v}_0^{(k)}}\left(\mathbf{h}_{\mathsf{d},i}^{(k)}\right) \end{bmatrix}_{\mathbf{s}^{(k)}=\mathbf{m}_i^{(k|k-1)}}, \quad (20)$$

where the generic elements in (20) are the derivatives of the measurement models in (14) with respect to the state, that is.

$$\nabla_{\mathbf{p}_0^{(k)}}\frac{\gamma}{2}\, d_j^{(\ell_k)} = \frac{\gamma}{2}\,\mathbf{a}_j^{(\ell_k)}\left(\phi_j^{(\ell_k)}, \theta_j^{(\ell_k)}\right), \quad (21)$$

$$\nabla_{\mathbf{p}_0^{(k)}}\phi_j^{(\ell_k)} = \mathbf{a}_j^{(\ell_k)}\left(\phi_j^{(\ell_k)}+\pi/2, \pi/2\right) / \left(d_j^{(\ell_k)}\,\sin\left(\theta_j^{(\ell_k)}\right)\right), \quad (22)$$

$$\nabla_{\mathbf{p}_0^{(k)}}\theta_j^{(\ell_k)} = \mathbf{a}_j^{(\ell_k)}\left(\phi_j^{(\ell_k)}, \theta_j^{(\ell_k)}+\pi/2\right) / \left(d_j^{(\ell_k)}\right), \quad (23)$$

$$\nabla_{\mathbf{v}_0^{(k)}}f_{\mathsf{d},j}^{(\ell_k)} = \frac{\gamma}{2\,\lambda}\,\mathbf{a}_j^{(\ell_k)}\left(\phi_j^{(\ell_k)}, \theta_j^{(\ell_k)}\right), \quad (24)$$

where $\mathbf{a}_j^{(\ell_k)} = \left[\mathsf{c}_{\phi,j}^{(\ell_k)}\,\mathsf{s}_{\theta,j}^{(\ell_k)}, \mathsf{s}_{\phi,j}^{(\ell_k)}\,\mathsf{s}_{\theta,j}^{(\ell_k)}, \mathsf{c}_{\theta,j}^{(\ell_k)}\right]^{\mathsf{T}}$ is the direction vector and where the following notation has been adopted: $\mathsf{c}_{\alpha,i}^{(k)} = \cos\left(\alpha_i^{(k)}\right)$, $\mathsf{s}_{\alpha,i}^{(k)} = \sin\left(\alpha_i^{(k)}\right)$ with $\alpha_i^{(k)}$ being the azimuth/elevation angle in the set $\left\{\phi_i^{(k)}, \theta_i^{(k)}\right\}$. Finally, we have

$$\nabla_{x_0^{(k)}}f_{\mathsf{d},j}^{(\ell_k)} = \frac{\gamma}{2\,\lambda}\left(-\mathsf{s}_{\phi,j}^{(\ell_k)}\,\mathsf{s}_{\theta,j}^{(\ell_k)}\,\omega_{\mathsf{z}} + \mathsf{c}_{\theta,j}^{(\ell_k)}\,\omega_{\mathsf{y}}\right), \quad (25)$$

$$\nabla_{y_0^{(k)}}f_{\mathsf{d},j}^{(\ell_k)} = \frac{\gamma}{2\,\lambda}\left(\mathsf{c}_{\phi,j}^{(\ell_k)}\,\mathsf{s}_{\theta,j}^{(\ell_k)}\,\omega_{\mathsf{z}} - \mathsf{c}_{\theta,j}^{(\ell_k)}\,\omega_{\mathsf{x}}\right), \quad (26)$$

$$\nabla_{z_0^{(k)}}f_{\mathsf{d},j}^{(\ell_k)} = \frac{\gamma}{2\,\lambda}\left(-\mathsf{c}_{\phi,j}^{(\ell_k)}\,\mathsf{s}_{\theta,j}^{(\ell_k)}\,\omega_{\mathsf{y}} + \mathsf{s}_{\phi,j}^{(\ell_k)}\,\mathsf{s}_{\theta,j}^{(\ell_k)}\,\omega_{\mathsf{x}}\right), \quad (27)$$

where the 3D angular velocity is given by

$$\boldsymbol{\omega}_i^{(k)} = \left[\omega_{\mathsf{x}},\, \omega_{\mathsf{y}},\, \omega_{\mathsf{z}}\right]^{\mathsf{T}} = \frac{\left(\mathbf{p}_0^{(k)}-\mathbf{p}_i^{(k)}\right)\times\left(\mathbf{v}_0^{(k)}-\mathbf{v}_i^{(k)}\right)}{\left(d_i^{(k)}\right)^2}, \quad (28)$$

where $\times$ indicates the cross product between the two vectors. If a measurement is not available (e.g., when a drone collects only ranging information), the correspondent row is eliminated from (20).

IV. INFORMATION-THEORETIC COST FUNCTION

The autonomous control in (6) is designed to estimate the next location of each UAV in order to maximize its capability to best track the target, considering also the locations and estimates of the neighboring UAVs. The tracking performance mainly depends on the prior information acquired (if present), on the UAV network formation (geometry) and on the uncertainty of the collected measurements.

In this section, we aim at deriving the analytical expression of the *information matrix* $\mathbf{J}_i^{(k)}(\cdot)$ in (7). Starting from the information model described in Sec. III-B and from the output of the EKF, it is possible to write the information matrix for the dynamic scenario as [26]

$$\mathbf{J}_i^{(k)}\left(\mathbf{p}_0^{(k)}; \mathbf{L}_i^{(k)}\right) = \\ = \left[\mathbf{P}_i^- - \mathbf{P}_i^-\,\nabla^{\mathsf{T}}\mathbf{h}_i^{(k)}\left(\mathbf{S}_i^{(k)}\right)^{-1}\nabla\mathbf{h}_i^{(k)}\,\mathbf{P}_i^-\right]_{11}^{-1}, \quad (29)$$

where $\mathbf{P}_i^- = \mathbf{P}_i^{(k|k-1)}$ is the predictive covariance, $\nabla^{\mathsf{T}}\mathbf{h}_i^{(k)}$ is the Jacobian matrix defined in (20), $\mathbf{S}_i^{(k)} = \nabla\mathbf{h}_i^{(k)}\,\mathbf{P}_i^-\,\nabla^{\mathsf{T}}\mathbf{h}_i^{(k)} + \mathbf{R}_i^{(k)}$, and $\mathbf{R}_i^{(k)}$ is the covariance matrix that depends on the statistical characterization of the measurement noise.

Then, according to the matrix inversion lemma [51], (29) can be reformulated in a more convenient form as

$$\mathbf{J}_i^{(k)}\left(\mathbf{p}_0^{(k)}; \mathbf{L}_i^{(k)}\right) = \left[\left(\mathbf{P}_i^-\right)^{-1} + \nabla^{\mathsf{T}}\mathbf{h}_i^{(k)}\left(\mathbf{R}_i^{(k)}\right)^{-1}\nabla\mathbf{h}_i^{(k)}\right]_{11} \\ = \mathbf{J}_{\mathsf{pp},i}^{(k|k-1)} + \mathbf{J}_{\mathsf{pp},i}^{(k|k)}, \quad (30)$$

where $\mathbf{J}_{\mathsf{pp},i}^{(k|k-1)} = \left[\left(\mathbf{P}_i^-\right)^{-1}\right]_{11}$ is the sub-block matrix corresponding to the predictive information matrix of the

$$\mathbf{J}_{\mathsf{pp},i}^{(k|k)}\left(\mathbf{p}_0^{(k)}; \mathbf{L}_i^{(k)}\right) = \sum_{j\in\left\{i,\mathcal{N}_{\mathsf{nb},i}^{(k)}\right\}} \mathrm{l}_j^{(\ell_k)}\left[\frac{\kappa_j}{\left(\sigma_{\mathsf{r},j}^{(\ell_k)}\right)^2}\mathbf{G}_{\mathsf{r},j}^{(\ell_k)}\left(\mathbf{p}_0^{(k)}; \mathbf{p}_j^{(\ell_k)}\right) + \frac{\xi_j}{\left(\sigma_{\mathsf{d},j}^{(\ell_k)}\right)^2}\mathbf{G}_{\mathsf{d},j}^{(\ell_k)}\left(\mathbf{p}_0^{(k)}; \mathbf{p}_j^{(\ell_k)}\right) \right. \\ \left. + \beta_j\left(\frac{1}{\left(\sigma_{\phi,j}^{(\ell_k)}\right)^2}\mathbf{G}_{\phi,j}^{(\ell_k)}\left(\mathbf{p}_0^{(k)}; \mathbf{p}_j^{(\ell_k)}\right) + \frac{1}{\left(\sigma_{\theta,j}^{(\ell_k)}\right)^2}\mathbf{G}_{\theta,j}^{(\ell_k)}\left(\mathbf{p}_0^{(k)}; \mathbf{p}_j^{(\ell_k)}\right)\right)\right], \quad (19)$$

target position, while $\mathbf{J}_{\mathsf{pp},i}^{(k|k)}$ corresponds to the FIM for non-random parameters, that is,

$$\mathbf{J}_{\mathsf{pp},i}^{(k|k)}\left(\mathbf{p}_0^{(k)};\mathbf{L}_i^{(k)}\right)=\nabla_{\mathbf{p}_0^{(k)}}^{\mathsf{T}}\mathbf{h}_i^{(k)}\left(\mathbf{R}_i^{(k)}\right)^{-1}\nabla_{\mathbf{p}_0^{(k)}}\mathbf{h}_i^{(k)}. \quad (31)$$

Equation (31) puts in evidence the relation of the information model $\left(\text{encapsulated in } \mathbf{R}_i^{(k)}\right)$ and of the UAV-target geometric configuration $\left(\text{in the Jacobian matrix, } \nabla_{\mathbf{p}_0^{(k)}}\mathbf{h}_i^{(k)}\right)$ on the localization performance. The deterministic FIM depends on the true target position and on the UAV locations as known by each UAV. Because this information is not available, they are substituted with their estimates. After some computation, it is possible to write the FIM in (31) as in (19), as shown at the bottom of the previous page, where κ_j is a flag equal to 1 if the jth neighbor of the ith UAV exchanges ranging information ($j \in \mathcal{N}_{\mathsf{r}} \vee \mathcal{N}_{\mathsf{j}}$, with $\vee$ being the *or*-operator), otherwise $\kappa_j = 0$; similarly β_j equals to 1 if the jth node can infer elevation and azimuth angles ($j \in \mathcal{N}_{\mathsf{b}} \vee \mathcal{N}_{\mathsf{j}}$), and, finally, $\xi_j = 1$ if Doppler shift measurements are available (i.e., if $j \in \mathcal{N}_{\mathsf{d}} \vee \mathcal{N}_{\mathsf{j}}$), otherwise $\xi_j = 0$. As we can see, (19) is composed of four main terms, each one carrying the position-related information from the corresponding measurements (ranging/bearing/Doppler). In turn, each term has a geometric component dependent on the UAV-target positions (the matrices $\mathbf{G}$) weighted by the measurement uncertainty (the factors $1/\sigma^2$). The latter are the inverse of the diagonal entries in the measurement covariance matrix $\mathbf{R}_i^{(k)}$, and are reported in (17). Thanks to the possibility to discriminate LOS/NLOS situations, we assume that the UAVs exactly know the values of the coefficients in (17).[5] The geometric matrices in (19) are given by

$$\begin{aligned}\mathbf{G}_{\mathsf{r},j}^{(\ell_k)}\left(\mathbf{p}_0^{(k)};\mathbf{p}_j^{(\ell_k)}\right)&=\frac{\gamma^2}{4}\nabla_{\mathbf{p}_0^{(k)}}^{\mathsf{T}}\left(d_j^{(\ell_k)}\right)\nabla_{\mathbf{p}_0^{(k)}}\left(d_j^{(\ell_k)}\right)\\&=\frac{\gamma^2}{4}\,\mathbf{a}_j^{(\ell_k)}\left(\mathbf{a}_j^{(\ell_k)}\right)^{\mathsf{T}},\end{aligned} \quad (32)$$

$$\begin{aligned}\mathbf{G}_{\phi,j}^{(\ell_k)}\left(\mathbf{p}_0^{(k)};\mathbf{p}_j^{(\ell_k)}\right)&=\nabla_{\mathbf{p}_0^{(k)}}^{\mathsf{T}}\left(\phi_j^{(\ell_k)}\right)\nabla_{\mathbf{p}_0^{(k)}}\left(\phi_j^{(\ell_k)}\right)\\&=\frac{\mathbf{G}_{\mathsf{r},j}^{(\ell_k)}\left(\phi_j^{(\ell_k)}+\pi/2,\pi/2\right)}{\left(d_j^{(\ell_k)}\sin\left(\theta_j^{(\ell_k)}\right)\right)^2},\end{aligned} \quad (33)$$

$$\begin{aligned}\mathbf{G}_{\theta,j}^{(\ell_k)}\left(\mathbf{p}_0^{(k)};\mathbf{p}_j^{(\ell_k)}\right)&=\nabla_{\mathbf{p}_0^{(k)}}^{\mathsf{T}}\left(\theta_j^{(\ell_k)}\right)\nabla_{\mathbf{p}_0^{(k)}}\left(\theta_j^{(\ell_k)}\right)\\&=\frac{\mathbf{G}_{\mathsf{r},j}^{(\ell_k)}\left(\phi_j^{(\ell_k)},\theta_j^{(\ell_k)}+\pi/2\right)}{\left(d_j^{(\ell_k)}\right)^2},\end{aligned} \quad (34)$$

$$\mathbf{G}_{\mathsf{d},j}^{(\ell_k)}\left(\mathbf{p}_0^{(k)};\mathbf{p}_j^{(\ell_k)}\right)=\frac{\gamma^2}{4\lambda^2}\nabla_{\mathbf{p}_0^{(k)}}^{\mathsf{T}}\left(f_{\mathsf{d},j}^{(\ell_k)}\right)\nabla_{\mathbf{p}_0^{(k)}}\left(f_{\mathsf{d},j}^{(\ell_k)}\right), \quad (35)$$

where the elements of (35) are reported in Appendix A.

When all the UAVs in $\mathcal{N}_{\mathsf{nb},i}^{(k)}$ are collecting non-informative or ambiguous measurements, for example when all the UAVs are in NLOS with the target ($\mathrm{l}_j^{(\ell_k)} = 0, \forall j$) or all have a malfunction in their processing capabilities ($\kappa_j = \beta_j = \xi_j = 0, \forall j$), they can rely on the previous state information to compute (30) and to perform the control task. In fact, in (30), when the measurement covariance matrix goes to zero (when σ^2 in (17) $\rightarrow \infty$), the only surviving term is the predictive information matrix $\mathbf{J}_{\mathsf{pp},i}^{(k|k-1)}$. The elements of (30) are given in Appendix B.

In the next section, a solution for the navigation problem in (6) is proposed based on a non-linear programming approach.

V. NAVIGATION ALGORITHM

To solve the trajectory problem in (6), one can rely on an approach based on optimization theory (e.g., non-linear programming [53]) or on a more advanced approaches of machine learning (e.g., reinforcement learning algorithms [30], dynamic programming [54] or based on approaches based on graph neural networks [55]).

One possibility to solve the minimization problem in (6) is to use a numerical approach. In the case study, we adopted the projection gradient method [39], [53]

$$\begin{aligned}\mathbf{u}_i^{(k+1)}=&-\nu\,\mathbf{M}\,\nabla_{\mathbf{p}_i^{(k)}}\mathcal{C}\left(\mathbf{J}_i^{(k)}\left(\hat{\mathbf{p}}_{0;i}^{(k)},\mathbf{L}_i^{(k)}\right)\right)\\&-\mathbf{N}\left(\mathbf{N}^{\mathsf{T}}\mathbf{N}\right)^{-1}\mathbf{g},\end{aligned} \quad (36)$$

where ν represents the spatial step, $\nabla_{\mathbf{p}_i^{(k)}}(\cdot)$ is the gradient operator with respect to the UAV positions which, taken with the negative sign, represents the direction of decrease of the cost function. The control signal computations are reported in Appendix C. The projection matrix is denoted with $\mathbf{M}=\mathbf{I}-\mathbf{N}\left(\mathbf{N}^{\mathsf{T}}\mathbf{N}\right)^{-1}\mathbf{N}^{\mathsf{T}}$ with $\mathbf{I}$ being the identity matrix and $\mathbf{N}=\left(\nabla_{\mathbf{p}_i^{(k)}}\mathbf{g}\right)$ being the gradient of the constraints in $\mathbf{g}=\left[\mathbf{g}_1^{\mathsf{T}}\ \mathbf{g}_2^{\mathsf{T}}\ \mathbf{g}_3^{\mathsf{T}}\right]^{\mathsf{T}}$, where

$$\mathbf{g}_1=\mathbf{d}_{\mathsf{U}}-d_{\mathsf{U}}^*,\quad \mathbf{d}_{\mathsf{U}}=\left\{d_{ij}^{(k)}:d_{ij}^{(k)}<d_{\mathsf{U}}^*\right\}, \quad (37)$$

$$\mathbf{g}_2=\mathbf{d}_{\mathsf{S}}-d_{\mathsf{T}}^*,\quad \mathbf{d}_{\mathsf{S}}=\left\{d_i^{(k)}:d_i^{(k)}<d_{\mathsf{T}}^*\right\}, \quad (38)$$

$$\mathbf{g}_3=\mathbf{d}_{\mathsf{O}}-d_{\mathsf{O}}^*,\quad \mathbf{d}_{\mathsf{O}}=\left\{d_{i,\mathsf{O}}^{(k)}:d_{i,\mathsf{O}}^{(k)}<d_{\mathsf{O}}^*\right\}. \quad (39)$$

Finally, we limit the UAV speed, altitude and the maximum turning rates according to (10).

The implemented tracking and navigation algorithms have a cubic complexity over the number of measurements available to a UAV at each time step. This number is the sum of the measurements from the neighbors and its own measurements. If the number of measurements surpasses the computational capacity of a UAV, it can decide to process only the most informative measurements or to select a subset of neighbors to collaborate with [41], [56]–[58]. A sketch on the computation complexity is reported in Appendix D.

VI. CASE STUDY

In this section, we analyze the performance of a DRN in different conditions: by changing the number of UAVs; by

[5]For example, this is possible if an electromagnetic map of the environment is available [52].

TABLE 1. RMSE [m] on target position for the configurations of Fig.4.

	$N=4$	$N=6$	$N=10$
Ranging-Only, $\sigma_{\mathrm{r},0}=10^{-4}$ m	0.53	0.33	0.15
Ranging-Only, $\sigma_{\mathrm{r},0}=10^{-2}$ m	1.55	0.82	0.64
Bearing-Only, $\sigma_{\mathrm{b},0}=5$ deg	1.38	0.85	0.82
Bearing-Only, $\sigma_{\mathrm{b},0}=20$ deg	3.85	2.27	1.55

varying their sensing capabilities; by dealing with different RCS; by varying the number of communication hops; and by operating in LOS-NLOS channel conditions. The investigated scenarios are displayed in Figs. 4-9, with environments covering more than one square kilometer.

In the simulations, the target mobility in (4) was modeled according to a constant velocity model with random accelerations [46], with

$$\mathbf{A}=\begin{bmatrix}\mathbf{I}_{3\times3} & \Delta t\,\mathbf{I}_{3\times3}\\ \mathbf{0}_{3\times3} & \mathbf{I}_{3\times3}\end{bmatrix},\ \mathbf{Q}=\begin{bmatrix}\frac{\Delta t^3}{3}\mathbf{W} & \frac{\Delta t^2}{2}\mathbf{W}\\ \frac{\Delta t^2}{2}\mathbf{W} & \Delta t\,\mathbf{W}\end{bmatrix}, \tag{40}$$

where $\mathbf{W}=\mathrm{diag}\left(w_{\mathrm{x}},\,w_{\mathrm{y}},\,w_{\mathrm{z}}\right)=\left(10^{-5},\,10^{-5},\,0\right)$ is a diagonal matrix containing the variances of the process noise in each direction. The number of UAVs and the target RCS were set to 6 and $0.1\,\mathrm{m}^2$, if not otherwise indicated. The safety distances, i.e., d^*_{U}, d^*_{T} and d^*_{O}, were all fixed at 5 m, the number of Monte Carlo iterations and the trajectory time steps at 100 and 3000 (each time step lasts 1 second), respectively. A communication range of 900 m between the UAVs and a single hop were considered [30], [59], if not otherwise indicated. We initialized the EKF as $\mathbf{m}_i^{(0)}=\mathbf{0}_{6\times1}$ and $\mathbf{P}_i^{(0)}=\mathrm{diag}\left(20^2\cdot\mathbf{I}_{3\times3},\,0.5^2\cdot\mathbf{I}_{3\times3}\right)$. The UAV minimum and maximum speed was set to $v_{\mathrm{min}}=0.5$ m/s, $v_{\mathrm{max}}=1$ m/s, respectively, and the maximum turning rate on azimuth and elevation planes as $\Psi_{\mathrm{max}}=\Theta_{\mathrm{max}}=50^\circ$ [29].

To compare the results, the success rate was evaluated as

$$\mathrm{SR}\left(e_{\mathrm{th}}\right)=\frac{1}{K\,N_{\mathrm{MC}}\,N}\sum_{k=1}^{K}\sum_{i=1}^{N}\sum_{m=1}^{N_{\mathrm{MC}}}\mathbf{1}\left(e_{\mathrm{th}}-e_{im}^{(k)}\right), \tag{41}$$

where N_{MC} is the number of Monte Carlo iterations, K is the number of time steps, $\mathbf{1}(x)$ is the unit step function that is equal to 1 if $x\geq0$ and 0 otherwise, $e_{im}^{(k)}$ is the estimation error of the target position at the ith UAV for the mth Monte Carlo iteration, where $e_{i,m}^{(k)}=\|\hat{\mathbf{p}}_{0;im}^{(k)}-\mathbf{p}_0^{(k)}\|_2$, and e_{th} is a localization threshold.

In the simulations of Fig. 4, the initial positions of UAVs were at the vertexes of a square lying on the XY-plane with $x_i^{(0)}=[-50,\,-50,\,500,\,500]^{\mathsf{T}}$ m, $y_i^{(0)}=[-50,\,500,\,-50,\,500]^{\mathsf{T}}$ m, and $z_i^{(0)}\sim\mathcal{U}\,[80,150]$ m, while the target initial position and velocity were $[0,0,90]^{\mathsf{T}}$ m and $[-0.3,0.4,0]^{\mathsf{T}}$ m/s.

In Fig. 4, we present qualitative examples of estimated UAV trajectories for different sensing capabilities (ranging and bearing) and considering $N=4$. The trajectories of UAVs are reported as blue lines and the positions are displayed with blue square markers for the initial and last time instants. The initial target position is drawn with a black triangle and its actual trajectory with a continuous black line. The estimated trajectory of the target is marked with a red dotted line. As can be seen, after an initial transient, the UAVs of the DRN jointly surround the target.

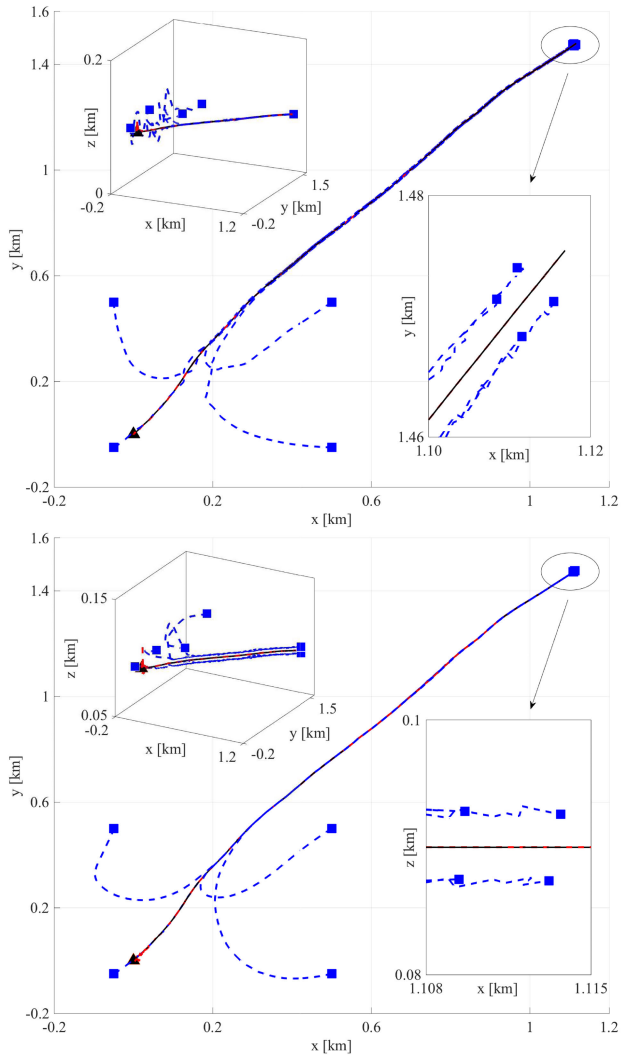

FIGURE 4. Simulated scenarios in LOS conditions with 4 UAVs estimating ranging information (top) with an accuracy $\sigma_{\mathrm{r},0}=10^{-4}$ m, and bearing information with an accuracy $\sigma_{\mathrm{b},0}=10^\circ$ deg. The initial positions and trajectory of the target and UAVs are indicated with black and blue lines, respectively. The estimated target trajectory is a dashed red line.

Given this scenario, in Table 1, we show the tracking performance in terms of average root mean squared error (RMSE) by varying the measurement accuracy and considering different number of UAVs. The RMSE on position and velocity was averaged over the number of discrete time instants and over the number of UAVs. A group of four radars with only ranging capability and accuracy of $\sigma_{\mathrm{r},0}=10^{-2}$ m obtains approximately the same tracking performance of four radars with only bearing capability and accuracy of about 5° degrees. Instead, when considering a better performing radar, such as the FMCW radar in [60]

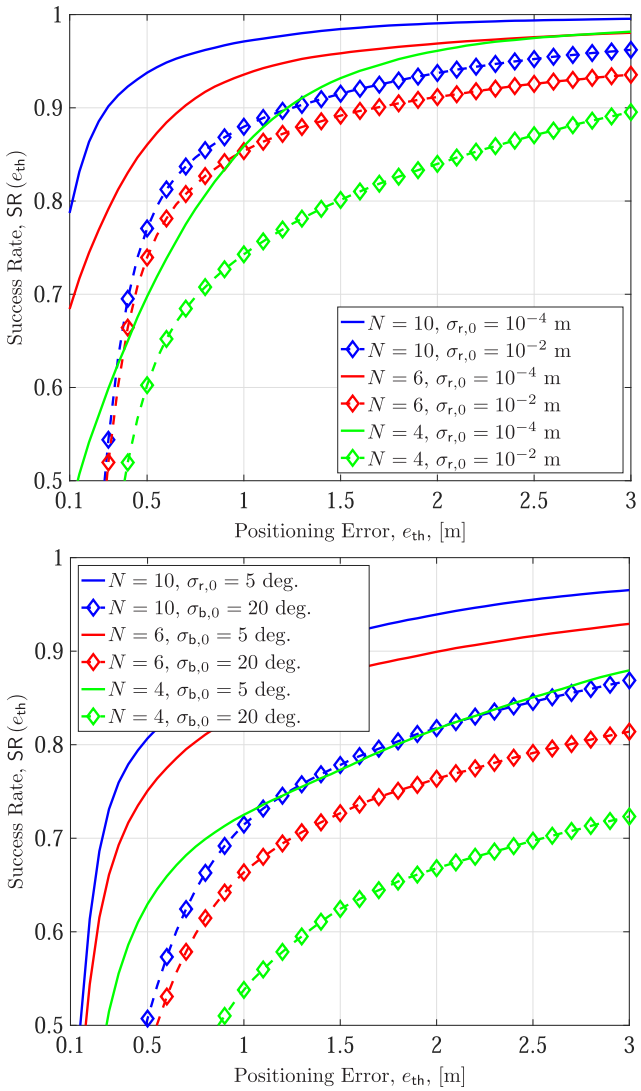

FIGURE 5. Success rate as a function of the number of UAVs for ranging (top) and bearing (bottom) measurements and different sensing accuracy.

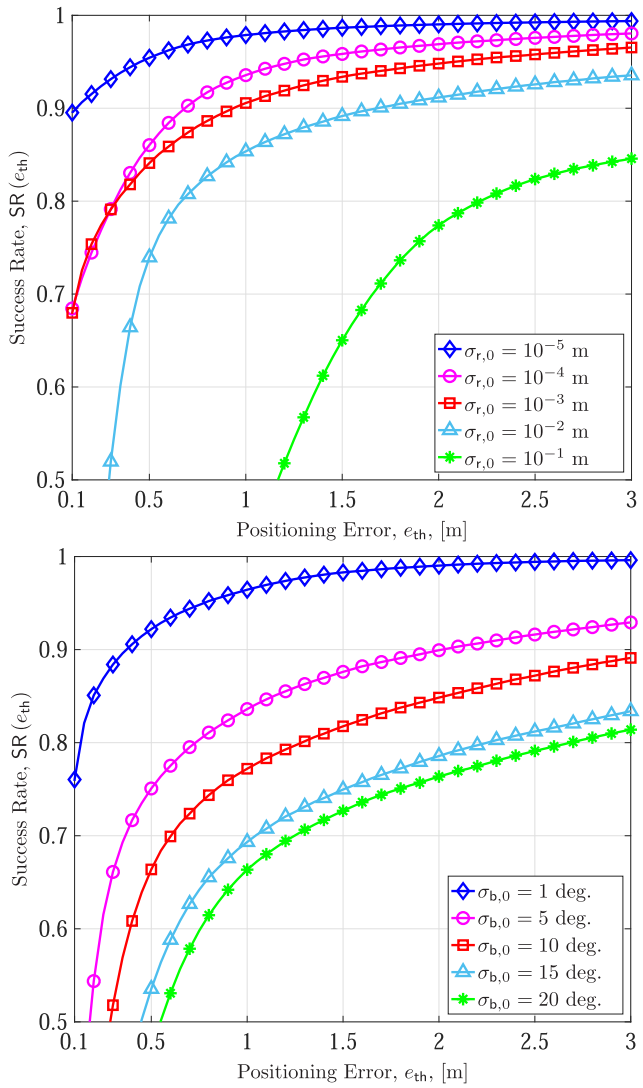

FIGURE 6. Success rate as a function of the ranging and bearing errors.

(i.e., with $\sigma_{\text{r},0} \approx 10^{-4}$ m), the average localization accuracy is below 1 m.

In Fig. 5, we provide the success rate evaluated as in (41) by varying the number of UAVs and the sensing capabilities. A localization error lower than 1 m can be achieved in nearly 80% of the cases with $N = 4$ UAVs with either a reference ranging accuracy of 10^{-2} m or a bearing accuracy of 5° degrees. This is also confirmed by Fig. 6 where several ranging and bearing errors were tested.

We now investigate the impact of the Doppler shifts and target RCS on the tracking performance with a fixed number of UAVs ($N = 6$). In Fig. 7-top, we show the success rate by considering ranging measurements and the presence of Doppler shifts with different chirp gains (i.e., $M_i = 64$-256) and different ranging accuracies. It can be observed that relying on Doppler shifts in addition to ranging measurements is beneficial especially when ranging is not sufficiently accurate: by fixing the desired localization error to 1 meter, the percentage increase experienced by adding Doppler shifts in the measurement vector is approximately of 100% with a ranging error of $\sigma_{\text{r},0} = 10^{-1}$ m (with $M_i = 256$, $\forall i = 1, \ldots, N$) whereas there are no evident improvements for $\sigma_{\text{r},0} = 10^{-3}$ m. Finally, in Fig. 7-bottom, we plot the success rate as a function of the target RCS. It is interesting to notice that a UAV with a RCS of 0.01 m can be localized in the 90% of cases with an error lower than 1 meter provided that a sensor with a ranging accuracy of 10^{-3} m is adopted.

In Fig. 8, we study the impact of a multi-hop exchange of measurements by limiting the number of temporal steps to $K = 500$ because the impact of multi-hops is more evident at the beginning of the trajectory. The ranging accuracy was $\sigma_{\text{r},0} = 10^{-3}$ m, the number of UAVs to $N = 4$, and a communication range of $r_{\text{max}} = 505$ m was considered. In Fig. 8-(top-left), the centralized case (the network is fully connected for all time instants, $r_{\text{max}} = \infty$) is reported as a benchmark. Fig. 8-(top-right) displays the single hop case with links depicted with grey lines, whereas in Fig. 8-(middle) the maximum number of hops was $h_{\text{max}} = 2$

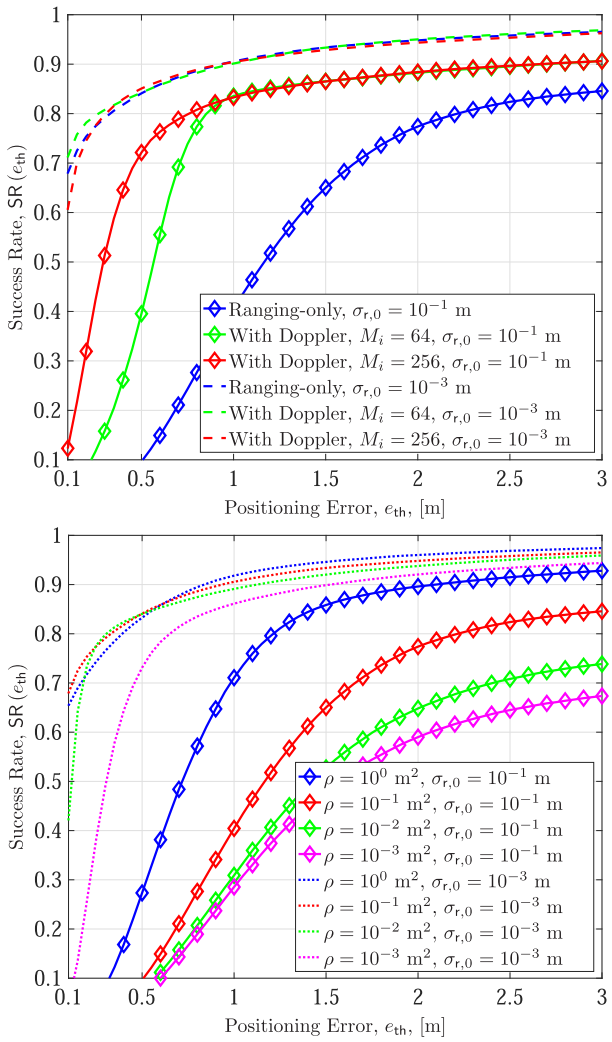

FIGURE 7. Success rate as a function of the positioning error when ranging measurements are collected. On the top, the case with and without Doppler shifts is considered for a ranging error of $\sigma_{r,0} = 10^{-3}$ m (dashed lines) and $\sigma_{r,0} = 10^{-1}$ m (diamond markers); on the bottom, the performance is compared as a function of the RCS.

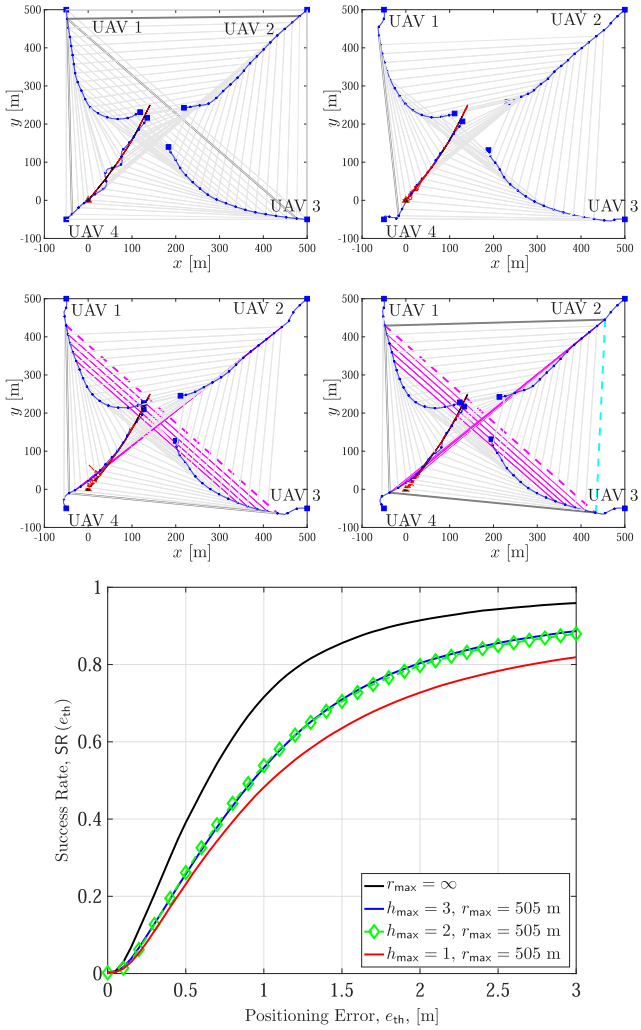

FIGURE 8. Plot of the first $K = 500$ instants of the trajectories with highlighted multi-hop connections. Top-left: Centralized case $r_{max} = \infty$ with links between UAVs depicted with grey lines. Top-right: Single-hop scenario ($h_{max} = 1$). Middle-left: Double-hop scenario ($h_{max} = 2$) with links reported with grey and magenta lines when a 1- or 2-hop is established, respectively. Middle-right: Triple-hop scenario ($h_{max} = 3$) with links reported with grey, magenta and cyan lines when a 1- or 2- or 3-hop is established, respectively. Bottom: Success rate as a function of the maximum number of hops.

(magenta lines) and 3 (cyan lines), respectively. For example, in Fig. 8-(top-right), UAV 1 is only connected with UAV 4 at time instant $k = 30$ because $h_{max} = 1$ and by having $r_{max} = 505$ m only UAV 4 is in the neighboring set of UAV 1. Contrarily, when $h_{max} = 2$, as in Fig. 8-(middle-left), it is also connected with UAV 3 through UAV 4. This means that the ranging information collected by UAV 3 will be available at UAV 1 after two time instants. Apart from an initial transient when the multi-hop propagation can be helpful as it allows to connect nodes otherwise unreachable, for the majority of the navigation time, a single-hop is sufficient thanks to the fact that the navigation control is conceived for minimizing the tracking error and, consequently, for minimizing the UAV-target and inter-UAVs distances. This is also confirmed from the results plotted in Fig. 8-(bottom) in terms of success rate.

At this point, we aim at comparing the performance of a DRN in presence of obstacles in order to assess the advantages of DRNs with respect to terrestrial fixed radar networks. To this purpose, we consider the scenario of Fig. 9 where obstacles are depicted with grey parallelepipeds, the UAVs composing the DRN with squared markers of different colors (every 500 time steps), and the terrestrial radars with squared blue markers. The ranging and bearing errors were 10^{-4} m and 5° degrees, respectively. In the DRN, the UAV initial positions were $x_i^{(0)} = [100,\ 100,\ 800,\ 800]^{\mathsf{T}}$ m, $y_i^{(0)} = [-1000,\ 300,\ 300,\ -1000]^{\mathsf{T}}$ m, and with a UAV height $z_i^{(0)} \sim \mathcal{U}[90, 150]$ m. The target altitude was set to 30 m, and its trajectory followed the dynamics described

TABLE 2. RMSE for the configurations of Fig.9.

	RMSE on position [m]		RMSE on velocity [m/s]	
	Terr. Rad.	Flying Rad.	Terr. Rad.	Flying Rad.
Ranging-Only	65.17	5.07	0.12	0.05
Bearing-Only	17.43	5.70	0.071	0.063

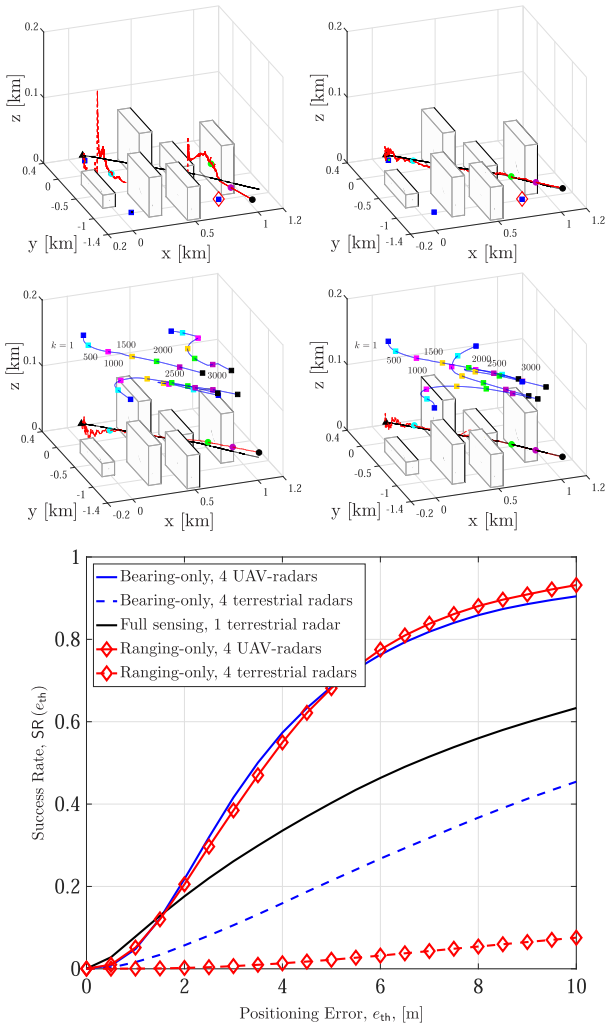

FIGURE 9. Simulated scenarios in NLOS conditions and success rate as a function of radar network configuration: comparison between terrestrial/fixed (top) and flying/dynamic (middle) radars for ranging (left) and bearing (right) processing capabilities, and success rate results (bottom).

by (40). For a better comparison, two situations with a fixed deployment of radar sensors were considered: one with a single terrestrial radar with full sensing capabilities (capable of retrieving ranging, bearing and Doppler shift information) represented with a red diamond in Fig. 9-top, and another where, for fairness of comparison, the fixed radar network is with the same number ($N = 4$) and sensing capabilities of UAVs. These radar configurations are compared in Fig. 9-bottom showing the superiority of a dynamic radar configuration over terrestrial networks in terms of success rate. Moreover, the RMSE results on position and velocity are reported in Table 2. In the case of a single terrestrial radar with full sensing capabilities, the RMSE on position and velocities is of 11.36 m and 0.06 m/s, respectively.

VII. CONCLUSION

In this paper, the idea of a UAV dynamic radar network for the tracking of a non-cooperative (e.g., unauthorized) UAV has been described. In contrast with current on-ground radar systems, the UAV network provides new degrees of freedom thanks to its reconfigurability and flexibility. Moreover, the UAVs are considered autonomous in navigating and estimating their best trajectory to minimize the tracking error of the dynamic target. The proposed network has heterogeneous sensing capabilities and estimates are shared among the UAVs. In this sense, the UAV cooperation can significantly increase the tracking accuracy without impacting the communication latency. The proposed control law aimed at minimizing an information-driven cost function derived starting from measurements and estimates exchanged by the UAVs at each time instant.

Results have demonstrated that having a flexible network instead of a terrestrial deployment of radars helps in preventing NLOS conditions and, thus, in better tracking a non-cooperative target. Moreover, even if the intruder is a small UAV (a target with RCS of 0.1 m^2 or less), the positioning performance is below 1 m most of the time, provided that a radar sensor with a millimeter ranging accuracy is available on-board, as for example a FMCW radar operating at 77 GHz. The same performance can be obtained with bearing measurements given an angular accuracy of about 5° degrees. Finally the use of Doppler shift estimates is beneficial to retrieve the velocity of the target instead of inferring it from position estimates. For this reason, the impact of the Doppler shift estimates is more valuable in the case where the ranging error is larger.

Future directions of research include the development of a control law able to maximize the expected information metric over a longer horizon (non-myopic approach) in order to deal better with complex and dynamic environments. Moreover, the scalability of the approach as a function of the number of UAVs, and in terms of computation time per each UAV, is important to investigate, especially for emergency applications where low latency is a very strict requirements. In this direction, clustering approaches can be adopted to separate the swarms of UAVs in sub-teams and reduce the "neighborhood of collaboration" of each UAV at the expense of reducing the accuracy of localization.

APPENDIX A

The elements in (35) provide the geometric matrix relative to Doppler shift measurements, and they are given by

$$\mathbf{G}_{\mathsf{d},j}^{(\ell_k)}\left(\mathbf{p}_0^{(k)},\mathbf{p}_j^{(\ell_k)}\right)=\left[\nabla_{\mathbf{p}_0^{(k)}}^{\mathsf{T}}\left(f_{\mathsf{d},j}^{(\ell_k)}\right)\ \nabla_{\mathbf{p}_0^{(k)}}\left(f_{\mathsf{d},j}^{(\ell_k)}\right)\right]_{\mathbf{s}^{(k)}=\mathbf{s}_0^-}$$
$$=\left(\frac{\gamma}{2\lambda}\right)^2\begin{bmatrix} g_{\mathsf{xx}} & g_{\mathsf{xy}} & g_{\mathsf{xz}}\\ g_{\mathsf{xy}} & g_{\mathsf{yy}} & g_{\mathsf{yz}}\\ g_{\mathsf{xz}} & g_{\mathsf{yz}} & g_{\mathsf{zz}}\end{bmatrix}, \tag{42}$$

with $\mathbf{s}_0^- = \hat{\mathbf{s}}_i^{(k|k-1)}$ and

$$g_{\mathsf{xx}}=\left(-\mathsf{s}_{\phi,j}^{(\ell_k)}\,\mathsf{s}_{\theta,j}^{(\ell_k)}\,\omega_{\mathsf{z}}+\mathsf{c}_{\theta,j}^{(\ell_k)}\,\omega_{\mathsf{y}}\right)^2,$$
$$g_{\mathsf{yy}}=\left(\mathsf{c}_{\phi,j}^{(\ell_k)}\,\mathsf{s}_{\theta,j}^{(\ell_k)}\,\omega_{\mathsf{z}}-\mathsf{c}_{\theta,j}^{(\ell_k)}\,\omega_{\mathsf{x}}\right)^2,$$
$$g_{\mathsf{zz}}=\left(-\mathsf{c}_{\phi,j}^{(\ell_k)}\,\mathsf{s}_{\theta,j}^{(\ell_k)}\,\omega_{\mathsf{y}}+\mathsf{s}_{\phi,j}^{(\ell_k)}\,\mathsf{s}_{\theta,j}^{(\ell_k)}\,\omega_{\mathsf{x}}\right)^2,$$

$$g_{\mathsf{xy}} = \left(-\mathsf{s}_{\phi,j}^{(\ell_k)}\,\mathsf{s}_{\theta,j}^{(\ell_k)}\,\omega_{\mathsf{z}} + \mathsf{c}_{\theta,j}^{(\ell_k)}\,\omega_{\mathsf{y}}\right)\left(\mathsf{c}_{\phi,j}^{(\ell_k)}\,\mathsf{s}_{\theta,j}^{(\ell_k)}\,\omega_{\mathsf{z}} - \mathsf{c}_{\theta,j}^{(\ell_k)}\,\omega_{\mathsf{x}}\right),$$
$$g_{\mathsf{xz}} = \left(\mathsf{s}_{\phi,j}^{(\ell_k)}\mathsf{s}_{\theta,j}^{(\ell_k)}\omega_{\mathsf{z}} - \mathsf{c}_{\theta,j}^{(\ell_k)}\omega_{\mathsf{y}}\right)\left(\mathsf{c}_{\phi,j}^{(\ell_k)}\mathsf{s}_{\theta,j}^{(\ell_k)}\omega_{\mathsf{y}} - \mathsf{s}_{\phi,j}^{(\ell_k)}\mathsf{s}_{\theta,j}^{(\ell_k)}\omega_{\mathsf{x}}\right),$$
$$g_{\mathsf{yz}} = \left(\mathsf{c}_{\phi,j}^{(\ell_k)}\mathsf{s}_{\theta,j}^{(\ell_k)}\omega_{\mathsf{z}} - \mathsf{c}_{\theta,j}^{(\ell_k)}\omega_{\mathsf{x}}\right)\left(-\mathsf{c}_{\phi,j}^{(\ell_k)}\mathsf{s}_{\theta,j}^{(\ell_k)}\omega_{y} + \mathsf{s}_{\phi,j}^{(\ell_k)}\mathsf{s}_{\theta,j}^{(\ell_k)}\,\omega_{\mathsf{x}}\right).$$

APPENDIX B

In this appendix, the elements of the *information matrix* in (30), that is,

$$\mathbf{J}_i^{(k)}\left(\mathbf{p}_0^{(k)};\mathbf{L}_i^{(k)}\right) = \begin{bmatrix} J_{\mathsf{xx},i} & J_{\mathsf{xy},i} & J_{\mathsf{xz},i} \\ J_{\mathsf{xy},i} & J_{\mathsf{yy},i} & J_{\mathsf{yz},i} \\ J_{\mathsf{xz},i} & J_{\mathsf{yz},i} & J_{\mathsf{zz},i} \end{bmatrix}, \tag{43}$$

are expanded in scalar notation. In particular, we have

$$\begin{aligned} J_{\mathsf{xx},i} = J_{\mathsf{xx},i}^{-} + \sum_{j\in\left\{i,\mathcal{N}_{\mathsf{nb},i}^{(k)}\right\}} \mathrm{l}_j^{(\ell_k)} \Bigg\{ & \frac{\kappa_j\,\gamma^2}{4\left(\sigma_{\mathsf{r},j}^{(\ell_k)}\right)^2}\left(\mathsf{c}_{\phi,j}^{(\ell_k)}\mathsf{s}_{\theta,j}^{(\ell_k)}\right)^2 \\ & + \frac{\beta_j}{\left(\sigma_{\mathsf{b},j}^{(\ell_k)}\,d_j^{(\ell_k)}\right)^2}\left[\left(\frac{\mathsf{s}_{\phi,j}^{(\ell_k)}}{\mathsf{s}_{\theta,j}^{(\ell_k)}}\right)^2 + \left(\mathsf{c}_{\phi,j}^{(\ell_k)}\,\mathsf{c}_{\theta,j}^{(\ell_k)}\right)^2\right] \\ & + \frac{\xi_j\,\gamma^2}{4\,\lambda^2\left(\sigma_{\mathsf{d},j}^{(\ell_k)}\right)^2}\,g_{\mathsf{xx}}\Bigg\}, \end{aligned} \tag{44}$$

$$\begin{aligned} J_{\mathsf{xy},i} = J_{\mathsf{xy},i}^{-} + \sum_{j\in\left\{i,\mathcal{N}_{\mathsf{nb},i}^{(k)}\right\}} \mathrm{l}_j^{(\ell_k)} \Bigg\{ & \frac{\kappa_j\,\gamma^2}{4\left(\sigma_{\mathsf{r},j}^{(\ell_k)}\right)^2}\,\mathsf{s}_{\phi,j}^{(\ell_k)}\,\mathsf{c}_{\phi,j}^{(\ell_k)}\left(\mathsf{s}_{\theta,j}^{(\ell_k)}\right)^2 \\ & + \frac{\beta_j}{\left(\sigma_{\mathsf{b},j}^{(\ell_k)}d_j^{(\ell_k)}\right)^2}\left[-\frac{\mathsf{s}_{\phi,j}^{(\ell_k)}\,\mathsf{c}_{\phi,j}^{(\ell_k)}}{\left(\mathsf{s}_{\theta,j}^{(\ell_k)}\right)^2} + \mathsf{s}_{\phi,j}^{(\ell_k)}\mathsf{c}_{\phi,j}^{(\ell_k)}\left(\mathsf{c}_{\theta,j}^{(\ell_k)}\right)^2\right] \\ & + \xi_j\,\frac{\gamma^2\,g_{\mathsf{xy}}}{4\,\lambda^2\left(\sigma_{\mathsf{d},j}^{(\ell_k)}\right)^2}\Bigg\}, \end{aligned} \tag{45}$$

$$\begin{aligned} J_{\mathsf{xz},i} = J_{\mathsf{xz},i}^{-} + \sum_{j\in\left\{i,\mathcal{N}_{\mathsf{nb},i}^{(k)}\right\}} \mathrm{l}_j^{(\ell_k)} \Bigg\{ & \frac{\kappa_j\,\gamma^2}{4\left(\sigma_{\mathsf{r},j}^{(\ell_k)}\right)^2}\,\mathsf{c}_{\phi,j}^{(\ell_k)}\,\mathsf{s}_{\theta,j}^{(\ell_k)}\,\mathsf{c}_{\theta,j}^{(\ell_k)} \\ & - \frac{\beta_j}{\left(\sigma_{\mathsf{b},j}^{(\ell_k)}\,d_j^{(\ell_k)}\right)^2}\,\mathsf{c}_{\phi,j}^{(\ell_k)}\,\mathsf{s}_{\theta,j}^{(\ell_k)}\,\mathsf{c}_{\theta,j}^{(\ell_k)} \\ & + \frac{\xi_j\,\gamma^2}{2\,\lambda^2\left(\sigma_{\mathsf{d},j}^{(\ell_k)}\right)^2}\,g_{\mathsf{xz}}\Bigg\}, \end{aligned} \tag{46}$$

$$\begin{aligned} J_{\mathsf{yy},i} = J_{\mathsf{yy},i}^{-} + \sum_{j\in\left\{i,\mathcal{N}_{\mathsf{nb},i}^{(k)}\right\}} \mathrm{l}_j^{(\ell_k)} \Bigg\{ & \kappa_j\frac{\gamma^2}{4\left(\sigma_{\mathsf{r},j}^{(\ell_k)}\right)^2}\left(\mathsf{s}_{\phi,j}^{(\ell_k)}\,\mathsf{s}_{\theta,j}^{(\ell_k)}\right)^2 \\ & + \beta_j\,\frac{1}{\left(\sigma_{\mathsf{b},j}^{(\ell_k)}\,d_j^{(\ell_k)}\right)^2}\left[\left(\frac{\mathsf{c}_{\phi,j}^{(\ell_k)}}{\mathsf{s}_{\theta,j}^{(\ell_k)}}\right)^2 + \left(\mathsf{s}_{\phi,j}^{(\ell_k)}\,\mathsf{c}_{\theta,j}^{(\ell_k)}\right)^2\right] \\ & + \xi_j\,\frac{\gamma^2}{4\,\lambda^2\left(\sigma_{\mathsf{d},j}^{(\ell_k)}\right)^2}\,g_{\mathsf{yy}}\Bigg\}, \end{aligned} \tag{47}$$

$$\begin{aligned} J_{\mathsf{zz},i} = J_{\mathsf{zz},i}^{-} + \sum_{j\in\left\{i,\mathcal{N}_{\mathsf{nb},i}^{(k)}\right\}} \mathrm{l}_j^{(\ell_k)} \Bigg\{ & \kappa_j\frac{\gamma^2}{4\left(\sigma_{\mathsf{r},j}^{(\ell_k)}\right)^2}\left(\mathsf{c}_{\theta,j}^{(\ell_k)}\right)^2 \\ & + \xi_j\,\frac{\gamma^2}{4\,\lambda^2\left(\sigma_{\mathsf{d},j}^{(\ell_k)}\right)^2}\,g_{\mathsf{zz}} \\ & + \beta_j\,\frac{1}{\left(\sigma_{\mathsf{b},j}^{(\ell_k)}\,d_j^{(\ell_k)}\right)^2}\left(\mathsf{s}_{\theta,j}^{(\ell_k)}\right)^2\Bigg\}, \end{aligned} \tag{48}$$

$$\begin{aligned} J_{\mathsf{yz},i} = J_{\mathsf{yz},i}^{-} + \sum_{j\in\left\{i,\mathcal{N}_{\mathsf{nb},i}^{(k)}\right\}} \mathrm{l}_j^{(\ell_k)} \Bigg\{ & \kappa_j\frac{\gamma^2}{4\left(\sigma_{\mathsf{r},j}^{(\ell_k)}\right)^2}\,\mathsf{s}_{\phi,j}^{(\ell_k)}\,\mathsf{c}_{\theta,j}^{(\ell_k)}\,\mathsf{s}_{\phi,j}^{(\ell_k)} \\ & + \xi_j\,\frac{\gamma^2}{4\,\lambda^2\left(\sigma_{\mathsf{d},j}^{(\ell_k)}\right)^2}\,g_{\mathsf{yz}} \\ & - \frac{\beta_j}{\left(\sigma_{\mathsf{b},j}^{(\ell_k)}\,d_j^{(\ell_k)}\right)^2}\,\mathsf{s}_{\phi,j}^{(\ell_k)}\,\mathsf{s}_{\theta,j}^{(\ell_k)}\,\mathsf{c}_{\theta,j}^{(\ell_k)}\Bigg\}. \end{aligned} \tag{49}$$

APPENDIX C

In this appendix, we derive the analytical expressions for control signals in (36). More specifically, we determine the term $\nabla_{\mathbf{p}_i^{(k)}}\mathcal{C}\left(\mathbf{J}_i^{(k)}\left(\hat{\mathbf{p}}_{0;i}^{(k)},\mathbf{L}_i^{(k)}\right)\right)$. According to (7), we have

$$\nabla_{\mathbf{p}_i^{(k)}}\mathcal{C}\left(\mathbf{J}_i^{(k)}\left(\hat{\mathbf{p}}_{0;i}^{(k)},\mathbf{L}_i^{(k)}\right)\right) = -\frac{\nabla_{\mathbf{p}_i^{(k)}}\left(\mathcal{D}_i^{(k)}\left(\mathbf{L}_i^{(k)}\right)\right)}{\mathcal{D}_i^{(k)}\left(\mathbf{L}_i^{(k)}\right)}, \tag{50}$$

where $\mathcal{D}_i^{(k)}\left(\mathbf{L}_i^{(k)}\right) = \det\left(\mathbf{J}_i^{(k)}\left(\hat{\mathbf{p}}_{0;i}^{(k)};\mathbf{L}_i^{(k)}\right)\right) = J_{\mathsf{xx},i}\,C_{\mathsf{xx}} + J_{\mathsf{xy},i}\,C_{\mathsf{yx}} + J_{\mathsf{xz},i}\,C_{\mathsf{zx}}$ is the determinant of the information matrix, and $C_{\mathsf{xx}} = J_{\mathsf{yy},i}J_{\mathsf{zz},i} - J_{\mathsf{zy},i}^2$, $C_{\mathsf{xy}} = C_{\mathsf{yx}} = J_{\mathsf{xz},i}J_{\mathsf{zy},i} - J_{\mathsf{xy},i}\,J_{\mathsf{zz},i}$, $C_{\mathsf{xz}} = C_{\mathsf{zx}} = J_{\mathsf{xy},i}J_{\mathsf{yz},i} - J_{\mathsf{xz},i}\,J_{\mathsf{yy},i}$, $C_{\mathsf{yy}} = J_{\mathsf{xx},i}\,J_{\mathsf{zz},i} - J_{\mathsf{xz},i}^2$, $C_{\mathsf{yz}} = J_{\mathsf{xz},i}\,J_{\mathsf{yx},i} - J_{\mathsf{xx},i}\,J_{\mathsf{yz},i}$, $C_{\mathsf{zz}} = J_{\mathsf{xx},i}\,J_{\mathsf{yy},i} - J_{\mathsf{xy},i}^2$ are the cofactors of the inverse. Consequently, the derivatives of the cost functions are

$$\begin{aligned} \nabla_{\mathbf{p}_i^{(k)}}\left(\mathcal{D}_i^{(k)}\left(\mathbf{L}_i^{(k)}\right)\right) = & \left(\nabla_{\mathbf{p}_i^{(k)}}J_{\mathsf{xx},i}\right)C_{\mathsf{xx}} \\ & + \left(\nabla_{\mathbf{p}_i^{(k)}}C_{\mathsf{xx}}\right)J_{\mathsf{xx},i} + \left(\nabla_{\mathbf{p}_i^{(k)}}J_{\mathsf{xy},i}\right)C_{\mathsf{yx}} \\ & + \left(\nabla_{\mathbf{p}_i^{(k)}}C_{\mathsf{yx}}\right)J_{\mathsf{xy},i} + \left(\nabla_{\mathbf{p}_i^{(k)}}J_{\mathsf{xz},i}\right)C_{\mathsf{zx}} \\ & + \left(\nabla_{\mathbf{p}_i^{(k)}}C_{\mathsf{xz}}\right)J_{\mathsf{zx},i}, \end{aligned} \tag{51}$$

where

$$\begin{aligned} \nabla_{\mathbf{p}_i^{(k)}}C_{\mathsf{xx}} = & \left(\nabla_{\mathbf{p}_i^{(k)}}J_{\mathsf{yy},i}\right)J_{\mathsf{zz},i} + \left(\nabla_{\mathbf{p}_i^{(k)}}J_{\mathsf{zz},i}\right)J_{\mathsf{yy},i} \\ & -2\,J_{\mathsf{zy},i}\left(\nabla_{\mathbf{p}_i^{(k)}}J_{\mathsf{zy},i}\right), \end{aligned} \tag{52}$$
$$\nabla_{\mathbf{p}_i^{(k)}}C_{\mathsf{yx}} = \left(\nabla_{\mathbf{p}_i^{(k)}}J_{\mathsf{xz},i}\right)J_{\mathsf{zy},i} + J_{\mathsf{xz},i}\left(\nabla_{\mathbf{p}_i^{(k)}}J_{\mathsf{zy},i}\right)$$

$$- \left(\nabla_{\mathbf{p}_i^{(k)}} J_{\mathsf{xy},i}\right) J_{\mathsf{zz},i} - J_{\mathsf{xy},i} \left(\nabla_{\mathbf{p}_i^{(k)}} J_{\mathsf{zz},i}\right), \quad (53)$$

$$\nabla_{\mathbf{p}_i^{(k)}} C_{\mathsf{xz}} = \left(\nabla_{\mathbf{p}_i^{(k)}} J_{\mathsf{xy},i}\right) J_{\mathsf{yz},i} + J_{\mathsf{xy},i} \left(\nabla_{\mathbf{p}_i^{(k)}} J_{\mathsf{yz},i}\right) - \left(\nabla_{\mathbf{p}_i^{(k)}} J_{\mathsf{xz},i}\right) J_{\mathsf{yy},i} - J_{\mathsf{xz},i} \left(\nabla_{\mathbf{p}_i^{(k)}} J_{\mathsf{yy},i}\right). \quad (54)$$

Starting from (49), it is straightforward to derive (54).

APPENDIX D

In this Appendix, we provide an analysis regarding the computational complexity at each UAV as a function of the number of neighboring UAVs for both the tracking and navigation algorithms. Obviously, increasing the number of sensing nodes is beneficial from a localization point-of-view. This has also been verified in the numerical results (e.g., in Fig. 5). At the same time, having a larger number of nodes implies a higher computational cost and time due to the increased number of measurements to be processed by each UAV and the number of safety constraints that can be simultaneously active. In the following, we show how the computational cost of each UAV at each time instant depends on the number of collaborative UAVs.

Let us assume that at some step k, N_{s} is the number of elements in the state vector and N_{m} is the number of measurements available at the generic ith UAV. Denote with N_{nb} the number of neighbors interacting with the UAV (here we drop the time index k and the UAV index i). The number of available measurements is $N_{\mathsf{m}} = \sum_{j \in \mathcal{N}_{\mathrm{nb}}} N_{\mathrm{m},j} + N_{\mathrm{m,o}}$, where $N_{\mathrm{m},j}$ is the number of measurements provided by the jth neighbor from the neighborhood $\mathcal{N}_{\mathrm{nb}}$, and $N_{\mathrm{m,o}}$ the number of own measurements. The maximum number of measurements generated by each UAV at each time instant is 4, i.e., range, Doppler shift and azimuth/elevation angles. Therefore, in this case the UAV has to process $N_{\mathrm{m}} = 4(N_{\mathrm{nb}} + 1)$ measurements.

We recall that each UAV runs two algorithms: (1) a target tracking algorithm using an EKF; (2) a navigation/formation algorithm using a projection gradient method. As described in Sec. III-C, the tracking algorithm is composed of two steps:

- *Prediction step*: The operations required for this step depend exclusively on the number of states (i.e., on N_{s}), and they are independent of the number of UAVs.
- *Update step*: The largest contribution to the computational cost of this step is the computation of the Kalman gain defined as

$$\mathbf{K} = \mathbf{P}^{-} \nabla^{\mathsf{T}} \mathbf{h} \, \mathbf{S}^{-1}, \quad (55)$$

$$\mathbf{S} = \nabla \mathbf{h} \, \mathbf{P}^{-} \nabla^{\mathsf{T}} \mathbf{h} + \mathbf{R}, \quad (56)$$

  where $\mathbf{P}^{-}$ is the predictive covariance matrix of the state, $\nabla \mathbf{h}$ is the observation Jacobian matrix, and $\mathbf{R}$ is the measurement noise covariance matrix. Therefore, the inversion of the $N_{\mathsf{m}} \times N_{\mathsf{m}}$ innovation covariance matrix $\mathbf{S}$ needs, in general, $\mathcal{O}(N_{\mathsf{m}}^3) = \mathcal{O}((4\,N_{\mathrm{nb}} + 4)^3)$ operations [61].

As regards the navigation control, the projection gradient algorithm in (36) requires the evaluation of the active constraints in (37) to form the projection matrix given by $\mathbf{M} = \mathbf{I} - \mathbf{N}\left(\mathbf{N}^{\mathsf{T}}\mathbf{N}\right)^{-1}\mathbf{N}^{\mathsf{T}}$. Consequently, also in this case, the most expensive operation in terms of sums and multiplications is the inversion of $\mathbf{N}^{\mathsf{T}}\mathbf{N}$, where the size of the constraint gradient $\mathbf{N}$ depends on the number of states and of active constraints in (37). In the worst case scenario, we have that the size of $\mathbf{g}_1$ (containing the distances from the neighboring UAVs with which a collision can happen) is N_{nb}, the size of $\mathbf{g}_2$ is 1, when the considered UAV is very close to the target, and the size of $\mathbf{g}_3$ depends only on the number of obstacles within the anti-collision sensors of the UAV. Therefore, the complexity of the navigation algorithm is $\mathcal{O}\left((N_{\mathrm{nb}} + 1)^3\right)$.

Consequently, the complexity of both algorithms depends on the number of neighbors N_{nb} of the UAV. Because the cost functions of the UAVs tend to keep the UAVs separated as much as possible, N_{nb} will be, in general, relatively small, and hence it is expected that the proposed distributed system easily scales with the number of UAVs without a significant increase of the computational complexity at each UAV.

REFERENCES

[1] N. Zhao, W. Lu, M. Sheng, Y. Chen, J. Tang, F. R. Yu, and K.-K. Wong, "UAV-assisted emergency networks in disasters," *IEEE Wireless Commun.*, vol. 26, no. 1, pp. 45–51, Feb. 2019.

[2] R. Shakeri, M. A. Al-Garadi, A. Badawy, A. Mohamed, T. Khattab, A. Al-Ali, K. A. Harras, and M. Guizani, "Design challenges of multi-UAV systems in cyber-physical applications: A comprehensive survey and future directions," *IEEE Commun. Surveys Tuts.*, vol. 21, no. 4, pp. 3340–3385, 4th Quart., 2019.

[3] M. Mozaffari, A. T. Z. Kasgari, W. Saad, M. Bennis, and M. Debbah, "Beyond 5G with UAVs: Foundations of a 3D wireless cellular network," vol. 18, no. 1, pp. 357–372, Jan. 2019.

[4] R. Gangula, P. de Kerret, O. Esrafilian, and D. Gesbert, "Trajectory optimization for mobile access point," in *Proc. 51st Asilomar Conf. Signals Sys. Comput.*, Oct. 2017, pp. 1412–1416.

[5] J. Chen, U. Yatnalli, and D. Gesbert, "Learning radio maps for UAV-aided wireless networks: A segmented regression approach," in *Proc. Int. Conf. Commun.*, May 2017, pp. 1–6.

[6] Y. Zeng, Q. Wu, and R. Zhang, "Accessing from the sky: A tutorial on UAV communications for 5G and beyond," *Proc. IEEE*, vol. 107, no. 12, pp. 2327–2375, Dec. 2019.

[7] W. Obile, "Ericsson mobility report," Ericsson, Stockholm, Sweden, Tech. Rep., 2016.

[8] I. Guvenc, F. Koohifar, S. Singh, M. L. Sichitiu, and D. Matolak, "Detection, tracking, and interdiction for amateur drones," *IEEE Commun. Mag.*, vol. 56, no. 4, pp. 75–81, Apr. 2018.

[9] F. Koohifar, I. Guvenc, and M. L. Sichitiu, "Autonomous tracking of intermittent RF source using a UAV swarm," *IEEE Access*, vol. 6, pp. 15884–15897, 2018.

[10] I. Bisio, C. Garibotto, F. Lavagetto, A. Sciarrone, and S. Zappatore, "Unauthorized amateur UAV detection based on WiFi statistical fingerprint analysis," *IEEE Commun. Mag.*, vol. 56, no. 4, pp. 106–111, Apr. 2018.

[11] P. Sarunic and R. Evans, "Hierarchical model predictive control of UAVs performing multitarget-multisensor tracking," *IEEE Trans. Aerosp. Electron. Syst.*, vol. 50, no. 3, pp. 2253–2268, Jul. 2014.

[12] P. Hügler, F. Roos, M. Schartel, M. Geiger, and C. Waldschmidt, "Radar taking off: New capabilities for UAVs," *IEEE Microw. Mag.*, vol. 19, no. 7, pp. 43–53, Nov./Dec. 2018.

[13] M. Ezuma, O. Ozdemir, C. K. Anjinappa, W. A. Gulzar, and I. Guvenc, "Micro-UAV detection with a low-grazing angle millimeter wave radar," in *Proc. Radio Wireless Symp.*, 2019, pp. 1–4.

[14] D. Casbeer, A. L. Swindlehurst, and R. Beard, "Connectivity in a UAV multi-static radar network," in *Proc. AIAA Guid. Navigat. Control Conf. Exhibit*, 2006, p. 6209.

[15] D. Solomitckii, M. Gapeyenko, V. Semkin, S. Andreev, and Y. Koucheryavy, "Technologies for efficient amateur drone detection in 5G millimeter-wave cellular infrastructure," *IEEE Commun. Mag.*, vol. 56, no. 1, pp. 43–50, Jan. 2018.

[16] B. Paul and D. W. Bliss, "Extending joint radar-communications bounds for FMCW radar with Doppler estimation," in *Proc. Radar Conf.*, May 2015, pp. 0089–0094.

[17] S. Schuster, S. Scheiblhofer, L. Reindl, and A. Stelzer, "Performance evaluation of algorithms for saw-based temperature measurement," *IEEE Trans. Ultrason., Ferroelectr., Freq. Control*, vol. 53, no. 6, pp. 1177–1185, Jun. 2006.

[18] Y. Liu, W. Li, Q. Lu, J. Wang, and Y. Shen, "Relative localization of ground vehicles using non-terrestrial networks," in *Proc. IEEE/CIC Int. Conf. Commun. Workshops China*, Aug. 2019, pp. 93–97.

[19] A. Guerra, D. Dardari, and P. Djuric, "Dynamic radar networks of UAVs: A tutorial overview and tracking performance comparison with terrestrial radar networks," *IEEE Veh. Technol. Mag.*, vol. 15, no. 2, pp. 113–120, Apr. 2020.

[20] A. Guerra, D. Dardari, and P. M. Djuric, "Non-centralized navigation for source localization by cooperative UAVs," in *Proc. 27th Eur. Signal Process. Conf.*, Sep. 2019, pp. 1–5.

[21] R. Feger, C. Wagner, S. Schuster, S. Scheiblhofer, H. Jager, and A. Stelzer, "A 77-GHz FMCW MIMO radar based on an SiGe single-chip transceiver," *IEEE Trans. Microw. Theory Techn.*, vol. 57, no. 5, pp. 1020–1035, May 2009.

[22] F. Folster, H. Rohling, and U. Lubbert, "An automotive radar network based on 77 GHz FMCW sensors," in *Proc. Int. Radar Conf.*, May 2005, pp. 871–876.

[23] F. Guidi, A. Guerra, and D. Dardari, "Personal mobile radars with millimeter-wave massive arrays for indoor mapping," *IEEE Trans. Mobile Comput.*, vol. 15, no. 6, pp. 1471–1484, Jun. 2016.

[24] F. Hoffmann, M. Ritchie, F. Fioranelli, A. Charlish, and H. Griffiths, "Micro-Doppler based detection and tracking of UAVs with multistatic radar," in *Proc. Radar Conf.*, May 2016, pp. 1–6.

[25] V. Semkin, J. Haarla, T. Pairon, C. Slezak, S. Rangan, V. Viikari, and C. Oestges, "Analyzing radar cross section signatures of diverse drone models at mmWave frequencies," *IEEE Access*, vol. 8, pp. 48958–48969, 2020.

[26] S. Martínez and F. Bullo, "Optimal sensor placement and motion coordination for target tracking," *Automatica*, vol. 42, no. 4, pp. 661–668, Apr. 2006.

[27] S. Ragi and E. K. P. Chong, "UAV path planning in a dynamic environment via partially observable Markov decision process," *IEEE Trans. Aerosp. Electron. Syst.*, vol. 49, no. 4, pp. 2397–2412, Oct. 2013.

[28] Z. M. Kassas and T. E. Humphreys, "Receding horizon trajectory optimization in opportunistic navigation environments," *IEEE Trans. Aerosp. Electron. Syst.*, vol. 51, no. 2, pp. 866–877, Jun. 2015.

[29] K. Doğançay, "UAV path planning for passive emitter localization," *IEEE Trans. Aerosp. Electron. Syst.*, vol. 48, no. 2, pp. 1150–1166, Apr. 2012.

[30] C. Wang, J. Wang, Y. Shen, and X. Zhang, "Autonomous navigation of UAVs in large-scale complex environments: A deep reinforcement learning approach," *IEEE Trans. Veh. Technol.*, vol. 68, no. 3, pp. 2124–2136, 2019.

[31] Y. Cai and Y. Shen, "An integrated localization and control framework for multi-agent formation," *IEEE Trans. Signal Process.*, vol. 67, no. 7, pp. 1941–1956, Feb. 2019.

[32] R. Opromolla, G. Inchingolo, and G. Fasano, "Airborne visual detection and tracking of cooperative UAVs exploiting deep learning," *Sensors*, vol. 19, no. 19, p. 4332, 2019.

[33] D. Ucinski, *Optimal Measurement Methods for Distributed Parameter System Identification*. Boca Raton, FL, USA: CRC Press, 2004.

[34] F. Meyer, H. Wymeersch, M. Fröhle, and F. Hlawatsch, "Distributed estimation with information-seeking control in agent networks," *IEEE J. Sel. Areas Commun.*, vol. 33, no. 11, pp. 2439–2456, Nov. 2015.

[35] F. Meyer, P. Braca, P. Willett, and F. Hlawatsch, "A scalable algorithm for tracking an unknown number of targets using multiple sensors," *IEEE Trans. Signal Process.*, vol. 65, no. 13, pp. 3478–3493, Jul. 2017.

[36] F. Meyer, O. Hlinka, H. Wymeersch, E. Riegler, and F. Hlawatsch, "Distributed localization and tracking of mobile networks including noncooperative objects," *IEEE Trans. Signal Inf. Process. Netw.*, vol. 2, no. 1, pp. 57–71, Mar. 2016.

[37] S. Tang and V. Kumar, "Autonomous flight," *Annu. Rev. Control, Robot., Auto. Syst.*, vol. 1, pp. 29–52, May 2018.

[38] G. Gu, P. R. Chandler, C. J. Schumacher, A. Sparks, and M. Pachter, "Optimal cooperative sensing using a team of UAVs," *IEEE Trans. Aerosp. Electron. Syst.*, vol. 42, no. 4, pp. 1446–1458, Oct. 2006.

[39] S. Zhang, R. Pohlmann, T. Wiedemann, A. Dammann, H. Wymeersch, and P. Hoeher, "Self-aware swarm navigation in autonomous exploration missions," *Proc. IEEE*, early access, May 7, 2020, doi: 10.1109/JPROC.2020.2985950.

[40] J. Wang, M. Garratt, A. Lambert, J. J. Wang, S. Han, and D. Sinclair, "Integration of GPS/INS/vision sensors to navigate unmanned aerial vehicles," *Int. Arch. Photogramm. Remote Sens. Spatial Info. Sci.*, vol. 37, no. part B1, pp. 963–969, 2008.

[41] N. Farmani, L. Sun, and D. J. Pack, "A scalable multitarget tracking system for cooperative unmanned aerial vehicles," *IEEE Trans. Aerosp. Electron. Syst.*, vol. 53, no. 4, pp. 1947–1961, Aug. 2017.

[42] D. Dardari, P. Closas, and D. M. Djuric, "Indoor tracking: Theory, methods, and technologies," *IEEE Trans. Veh. Technol.*, vol. 64, no. 4, pp. 1263–1278, Apr. 2015.

[43] J. T. Isaacs, F. Quitin, L. R. G. Carrillo, U. Madhow, and J. P. Hespanha, "Quadrotor control for RF source localization and tracking," in *Proc. Int. Conf. Unmanned Aircr. Syst.*, May 2014, pp. 244–252.

[44] A. Guerra, D. Dardari, and P. M. Djurić, "Joint indoor localization and navigation of UAVs for network formation control," in *Proc. 52nd Asilomar Conf. Signals Sys. Comput.*, Oct. 2018, pp. 13–19.

[45] S. Xu, K. Doğançay, and H. Hmam, "3D AOA target tracking using distributed sensors with multi-hop information sharing," *Signal Process.*, vol. 144, pp. 192–200, Mar. 2018.

[46] S. Särkkä, *Bayesian Filtering and Smoothing*, vol. 3. Cambridge, U.K.: Cambridge Univ. Press, 2013.

[47] K. Dedecius and P. M. Djurić, "Sequential estimation and diffusion of information over networks: A Bayesian approach with exponential family of distributions," *IEEE Trans. Signal Process.*, vol. 65, no. 7, pp. 1795–1809, Apr. 2017.

[48] I. Ivashko, O. Krasnov, and A. Yarovoy, "Performance analysis of multisite radar systems," in *Proc. Eur. Radar Conf.*, Oct. 2013, pp. 459–462.

[49] I. M. Ivashko, O. A. Krasnov, and A. G. Yarovoy, "Topology optimization of monostatic radar networks with wide-beam antennas," in *Proc. Eur. Radar Conf.*, Sep. 2015, pp. 133–136.

[50] M. Petitjean, S. Mezhoud, and F. Quitin, "Fast localization of ground-based mobile terminals with a transceiver-equipped UAV," in *Proc. 29th Annu. Int. Symp. Pers., Indoor, Mobile Radio Commun.*, Sep. 2018, pp. 323–327.

[51] Y. Bar-Shalom, X. R. Li, and T. Kirubarajan, *Estimation With Applications to Tracking and Navigation: Theory Algorithms and Software*. Hoboken, NJ, USA: Wiley, 2004.

[52] D. Dardari, E. Falletti, and M. Luise, *Satellite and Terrestrial Radio Positioning Techniques: A Signal Processing Perspective*. Amsterdam, The Netherlands: Elsevier, 2012.

[53] D. G. Luenberger and Y. Ye, *Linear and Nonlinear Programming*, vol. 2. Reading, MA, USA: Addison-Wesley, 1984.

[54] D. P. Bertsekas, *Dynamic Programming and Optimal Control*, vol. 1, no. 2. Belmont, MA, USA: Athena scientific, 1995.

[55] J. Fink, A. Ribeiro, and V. Kumar, "Robust control of mobility and communications in autonomous robot teams," *IEEE Access*, vol. 1, pp. 290–309, 2013.

[56] S. Hadzic and J. Rodriguez, "Utility based node selection scheme for cooperative localization," in *Proc. Int. Conf. Indoor Positioning Navig.*, Sep. 2011, pp. 1–6.

[57] F. Meyer, B. Etzlinger, Z. Liu, F. Hlawatsch, and M. Z. Win, "A scalable algorithm for network localization and synchronization," *IEEE Internet Things J.*, vol. 5, no. 6, pp. 4714–4727, Dec. 2018.

[58] R. M. Buehrer, H. Wymeersch, and R. M. Vaghefi, "Collaborative sensor network localization: Algorithms and practical issues," *Proc. IEEE*, vol. 106, no. 6, pp. 1089–1114, Jun. 2018.

[59] Y. Wang, Y. Wu, and Y. Shen, "Cooperative tracking by multi-agent systems using signals of opportunity," *IEEE Trans. Commun.*, vol. 68, no. 1, pp. 93–105, Jan. 2020.

[60] *IWR1443 Single-Chip 76-GHz to 81-GHz mmWave Sensor*. Accessed: Jun. 2020. [Online]. Available: http://www.ti.com/lit/wp/spyy005/spyy005.pdf

[61] J. Mendel, "Computational requirements for a discrete Kalman filter," *IEEE Trans. Autom. Controlol*, vol. 16, no. 6, pp. 748–758, Dec. 1971.

ANNA GUERRA (Member, IEEE) received the B.S. and M.S. degrees in electronics and telecommunications engineering and the Ph.D. degree in electronics, telecommunications, and information technologies from the University of Bologna (UNIBO), in 2009, 2011, and 2016, respectively. Since 2016, she has been a Postdoctoral Researcher with the University of Bologna. In 2012, she was a Research Assistant in a collaboration project between the Italian National Inter-University Consortium for Telecommunications and the French Atomic Energy Commission (CEA-LETI), Grenoble, France. From 2014 to 2015, she was a Visiting Student at CEA-LETI. She was a recipient of the H2020 IF-GF Marie Skłodowska-Curie Fellowship (AirSens project) in collaboration between UNIBO and Stony Brook University, Stony Brook, NY, USA, in 2018. She received the Best Student Paper Award at the 2014 IEEE International Conference on Ultra-Wideband held in Paris, France, and the Best Paper Award at the 2019 IEEE RFID-TA Conference, Pisa, Italy. She serves as a reviewer for numerous IEEE journals and international conferences.

DAVIDE DARDARI (Senior Member, IEEE) is currently an Associate Professor at the University of Bologna, Italy. Since 2005, he has been a Research Affiliate at the Massachusetts Institute of Technology, USA. His research interests include wireless communications, localization techniques, and distributed signal processing. He published more than 200 technical articles and held several important roles in various national and European projects.

He received the IEEE Aerospace and Electronic Systems Society's M. Barry Carlton Award, in 2011, and the IEEE Communications Society Fred W. Ellersick Prize, in 2012. He was the Chair of the Radio Communications Committee of the IEEE Communication Society and a Distinguished Lecturer from 2018–2019. He was the Co-General Chair of the 2011 IEEE International Conference on Ultra-Wideband and a Co-Organizer of the IEEE International Workshop on Advances in Network Localization and Navigation (ANLN) - ICC 2013-2016 editions. He was also the TPC Chair of the IEEE International Symposium on Personal, Indoor and Mobile Radio Communications (PIMRC 2018), the TPC Co-Chair of the Wireless Communications Symposium of the 2007/2017 IEEE International Conference on Communications and the 2006 IEEE International Conference on Ultra-Wideband. He served as an Editor for the IEEE Transactions on Wireless Communications from 2006 to 2012, and as a guest editor for several journals.

PETAR M. DJURIĆ (Fellow, IEEE) received the B.S. and M.S. degrees in electrical engineering from the University of Belgrade, Belgrade, Yugoslavia, and the Ph.D. degree in electrical engineering from the University of Rhode Island, Kingston, RI, USA. He is a SUNY Distinguished Professor and currently a Chair of the Department of Electrical and Computer Engineering, Stony Brook University, Stony Brook, NY, USA. His research interests include the area of signal and information processing with primary interests in the theory of Monte Carlo-based methods, Bayesian machine learning, signal modeling, detection, and estimation, signal and information processing over networks, RFID, and the IoT. Recently, his research has been applied to problems related to machine learning methods for intrapartum fetal monitoring and brain signals. He has been invited to lecture at many universities in U.S. and overseas. He is a Fellow of EURASIP. He was a recipient of the *IEEE Signal Processing Magazine* Best Paper Award, in 2007, and the EURASIP Technical Achievement Award, in 2012. In 2008, he was the Chair of Excellence of the Universidad Carlos III de Madrid-Banco de Santander. From 2008 to 2009, he was a Distinguished Lecturer of the IEEE Signal Processing Society. He has been on numerous committees of the IEEE Signal Processing Society and of many professional conferences and workshops. He was the Editor-in-Chief of the IEEE Transactions on Signal and Information Processing Over Networks.